Università degli Studi di Padova

Dipartimento di Ingegneria Industriale
Corso di Laurea in Ingegneria Aerospaziale

Tesi di Laurea Magistrale

Development of a surrogate model of a FSAE car based on DOE techniques

Relatore:
Prof. Ernesto Benini

Laureando:
Riccardo Milan

Correlatore:
Ing. Andrea Dal Monte

Anno accademico 2017 / 2018

Nomenclature

A $[m^2]$	Section area	V $[m/s]$	Velocity
c $[m]$	Chord length	p $[Pa]$	Static pressure
C_l $[-]$	Lift coefficient	μ $[m^2 s]$	Dynamic viscosity
C_d $[-]$	Drag coefficient	L $[m]$	Characteristic length
Re $[-]$	Reynolds number	$y+$ $[-]$	Adimensional wall distance
ρ $[kg/m^3]$	Fluid density		

Contents

1 The Formula SAE 1
- 1.1 What is Formula SAE . . . 1
- 1.2 The event . . . 1
  - 1.2.1 Technical inspections . . . 2
  - 1.2.2 Static Events . . . 3
  - 1.2.3 Dynamic Events . . . 3
- 1.3 The Race UP Team . . . 5

2 Car Aerodynamics 7
- 2.1 Aerodynamic forces . . . 7
  - 2.1.1 Drag . . . 8
  - 2.1.2 Lift . . . 10
- 2.2 Forces effect . . . 11
  - 2.2.1 Wings . . . 12
  - 2.2.2 Undertray . . . 15

3 CFD 17
- 3.1 Mathematical model . . . 17
- 3.2 The process . . . 18
  - 3.2.1 Pre-processing . . . 18
  - 3.2.2 Solver . . . 26
  - 3.2.3 Post-Processing . . . 27

4 Experimental test 29
- 4.1 Sensors set-up . . . 29
- 4.2 The test . . . 31
- 4.3 Data analysis . . . 33

5 Validation 39
- 5.1 Simulation set-up . . . 39
- 5.2 Geometry preparation . . . 40
- 5.3 Starting geometry . . . 41
- 5.4 First Attempt . . . 43
- 5.5 Second Attempt . . . 46
- 5.6 Third Attempt . . . 48
- 5.7 Fourth Attempt . . . 50
- 5.8 Fifth Attempt . . . 51
- 5.9 Sixth Attempt . . . 54
  - 5.9.1 Mesh sensitivity analysis . . . 55
- 5.10 Seventh Attempt . . . 55

5.10.1 Unsteady analysis 57
5.10.2 Mesh Sensitivity 59
5.11 Other configurations 61

6 Design of experiments 63
6.1 Variables choice 63
6.2 DOE set-up 65
6.2.1 DOE results 66
6.3 Aerodynamic balance 69
6.3.1 Center of Pressure 69
6.3.2 Load distribution 71

7 Conclusions 75

LIST OF FIGURES

1.1 Tilt test. 2
1.2 Track for the Skid-Pad event[1]. 4
1.3 FSAE Germany Autocross track (2012). 4

2.1 Chaparral 2e (1966) 7
2.2 Aerodynamic forces [2] 8
2.3 Example of flow detachment caused by body shape [3] 9
2.4 Trend of cp and velocity along a body [3] 10
2.5 Velocity profile inside the boundary layer [3] 10
2.6 Boundary Layer transition 11
2.7 Relation between friction coefficient and *Re* [2] 11
2.8 Airfoil[2] 12
2.9 Airfoil 13
2.10 Cl and Cd 13
2.11 Gurney flap [4] 14
2.12 Underbody working principle [4] 15

3.1 Different types of element shape [5] 20
3.2 Prismatic mesh for the boundary layer 21
3.3 Cell growth rate [5] 21
3.4 Different types of mesh quality index [5] 22
3.5 Boundary Layer development [6] 23
3.6 Law of the wall [7] 25
3.7 CFD physical phenomena summary 26

4.1 MG X.15 29
4.2 Rear wing attachment system 30
4.3 Load cell 30
4.4 Final set-up 31
4.5 Relative distance and angles 32
4.6 Configurations tested 33
4.7 Angles for the decomposition 33
4.8 Example of acquisition output 34

5.1 CFD domain 40
5.2 Original CAD and CFD CAD 41
5.3 Original CAD and CFD CAD 42
5.4 Original mesh 43
5.5 Modified elements 44
5.6 Squared trailing edge 44
5.7 First attempt mesh 44

5.8 $y+$ distribution on the rear wing 45
5.9 First attempt mesh 46
5.10 Second attempt rear wing $y+$ 47
5.11 Second attempt velocity scalar field 47
5.12 Second attempt residuals 48
5.13 Second attempt downforce 48
5.14 Third attempt mesh with wake refinement 49
5.15 Third attempt velocity scalar field 49
5.16 Rear wing with gurney 50
5.17 Detail of velocity scalar field near gurney 51
5.18 Modified geometry with firewall 51
5.19 Volumetric refinement 52
5.20 Volumetric refinement at the gurney 52
5.21 Fifth Attempt mesh 53
5.22 Velocity scalar field at the gurney 53
5.23 Sixth attempt mesh 54
5.24 Final mesh 56
5.25 Seventh attempt residuals 57
5.26 Seventh attempt forces 57
5.27 Y-Velocity field in the wake region 58
5.28 Unsteady analysis residuals 59
5.29 Unsteady analysis forces 59
5.30 Mesh sensitivity trend curve 60

6.1 Front wing: in red the central flaps, in blue the lateral flaps 63
6.2 Example of flap rotation 64
6.3 Aerodynamic configurations 64
6.4 Nine-points grid for the DOE 65
6.5 Downforce response surface 67
6.6 Drag response surface 67
6.7 Efficiency response surface 68
6.8 Comparison between understeer and oversteer 70
6.9 COG position 71
6.10 Example of COP line 71
6.11 Definition of the COP 72
6.12 Load distribution response surface 73

List of Tables

3.1 Difference between compressible and incompressible 22

4.1 Relative distances and angles 32
4.2 Acceleration set-up 35
4.3 Medium load configuration 35
4.4 High load configuration 35
4.5 Final results 36

5.1 Refinements used 42
5.2 Original mesh results 43
5.3 Sensitivity analysis results 55
5.4 Results unsteady analysis 58
5.5 Results from different configurations 61

6.1 Absolute flap inclination for different configurations 65
6.2 DOE results 66
6.3 Load distribution for all the nine points 72

SUMMARY

Nowadays the aerodynamic design for racecar is very important and it becomes necessary in order to reach the maximum performance. The FSAE is an engineering student competition: its goal is to give the possibility to create a small formula car, designed and made entirely by students. Even in this kind of competition the development of a complete aeropack is currently essential. Experimental tests are complex to perform and for this reason the most common instrument for the aerodynamic design is the computational fluid dynamics (CFD). CFD allows to simulate complicated geometry in a reasonable amount of time, but the model, in terms of geometry and mesh, must be validated comparing the results from the CFD with experimental data. The main focus of this thesis is the creation and validation of a CFD model of the MG X.15, a FSAE car of the University of Padova, using the results obtained from experimental tests carried on the rear wing. In the second part was developed a surrogate model of the MG 13.18 based on a DOE analysis. The DOE utilizes a multiple points grid to explore the solution space; the variables used for the research are the relative inclinations between front and rear wing flaps. The results are used to create a response surface and evaluate the influence of the variables on the aerodynamic performance in order to create the basis for an active control.

- I -

THE FORMULA SAE

1.1 WHAT IS FORMULA SAE

The Formula SAE is a student competition organized by the Society of Automotive Engineers (SAE) which involves the design and production of a racing car, evaluated during a series of tests based on its design quality and engineering efficiency. The idea behind the Formula SAE is that a fictitious company hires the team to make a prototype racing car with certain characteristics. Each team of students must design, build, test and promote the prototype, which is evaluated in eight tests, from pure performance, to the business plan and the presentation of the vehicle itself. For each event it is possible to total a maximum of 1000 points distributed among various tests according to the following scheme:

Events	
Business Plan Presentation	75
Engineering Design	150
Cost Analysis	100
Acceleration	100
Skid-Pad	75
Autocross	125
Fuel economy	100
Endurance	275
Total Points	1000

1.2 THE EVENT

Each FSAE event consists of four days of competition in some of the most famous and important world tracks. All the events, which take place worldwide, have the same regulation, but each constitute an independent competition without contributing to award points for a championship. The first FSAE event took place in 1980 in the United States and, since then, more than 450 Universities from all over the world have participated at least at one race.

In order to compete the cars must comply with a precise regulation, above all aimed at guaranteeing safety and limiting their performance, giving the chance for new technical solutions.

For example, the engine has a constraint on the displacement (710 cc) and a 20 mm diameter restriction on the intake circuit.

The car must provide adequate protection for the driver in the event of a side impact or overturning; furthermore, an impact absorption system must be placed in the front part of the car to absorb energy in the event of frontal collision.

1.2.1 Technical inspections

Before being able to run the vehicle, every car is subjected to a series of checks and inspections by the judges, who verify compliance with the regulation, especially regarding the rules that ensure the safety of the pilot.

After the inspection, the vehicle is refilled and it is positioned on the tilt table, a platform able to tilt the prototype on both sides, up to an angle of 60 degrees, in order to certify that there is no loss of liquids.

Then the car undergoes the noise check, in which the judges verify that the engine, running at different speeds, does not exceed 110 dB of noise. The last of the pre-race controls is the braking test, in which the car must be able, after a long acceleration, to lock all four wheels at the same time.

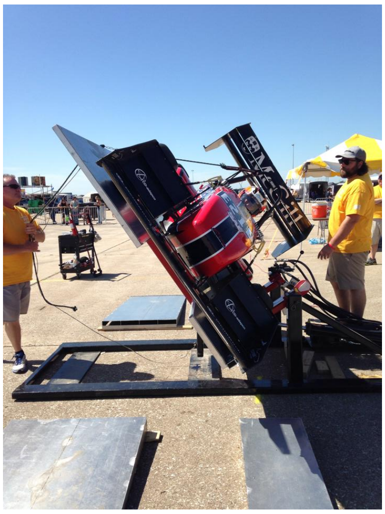

Figure 1.1: *Tilt test.*

1.2.2 STATIC EVENTS

Cost Analysis

The test is divided into two parts: the compilation of a written report, which must be sent to the judges before the competition, and a discussion during the event itself. This allows to evaluate not only the cost of the prototype, but also the team's ability to produce an accurate estimate of production and design costs. It is therefore clear that the cost report must correspond to the car chosen for the competition. The car with the lowest purchase cost and the one with the best presentation receive 30 points each. During the event another 20 points are given to reward the real possibility of producing the vehicle, while the last 20 points are awarded to the team exposition about the production processes on two subjects chosen at random by the judges.

Business Plan Presentation

This presentation is designed to assess the team's ability to develop and deliver a large and comprehensive business case.

Engineering Design

The idea behind this event is to evaluate the design choices and efforts. These aspects are evaluated by the judges in an interview with each team.

1.2.3 DYNAMIC EVENTS

Acceleration

During the acceleration test the car must accelerate for 75 meters along a straight path on a flat surface. The test is divided into four attempts, which must be run by two different drivers. The score is determined by the difference between the worst and the best absolute time recorded.

Skid-Pad

The test evaluates the car ability during the cornering phase. The track is similar to an eight shape with two circles of 15.25 meters. Once the vehicle has entered the path, it must run along the right circle two times, where the second one is considered for the test time. After the second lap, the car must move to the left circle to make two more laps. After the fourth lap, the car leaves the track. The test is divided into two batteries, which must be run by two different drivers, each of which has two attempts. The score is determined on the average time of the two measured laps.

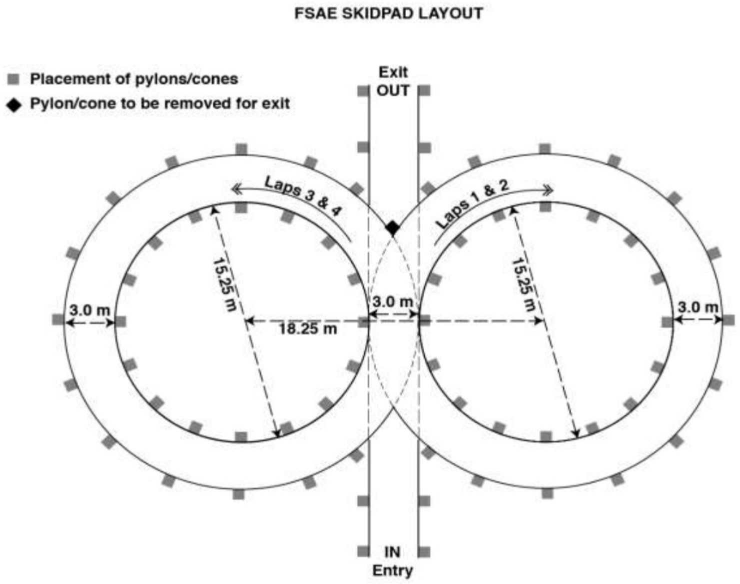
FSAE SKIDPAD LAYOUT
Placement of pylons/cones
Pylon/cone to be removed for exit
Exit
OUT
Laps 3 & 4
Laps 1 & 2
15.25 m
15.25 m
3.0 m
3.0 m
3.0 m
18.25 m
IN
Entry

Figure 1.2: *Track for the Skid-Pad event[1].*

Autocross

The goal of the autocross event is to evaluate the car manoeuvrability and handling qualities on a tight track without the hindrance of other competing cars. The autocross combines the performance features of acceleration, braking, and cornering into one event. Each car has to complete at least one lap and the resulting time lap is considered for the score. The track is designed to obtain average speeds of 40/50 km/h and includes short straights (no more than 60 m), turns with constant radius (from 23 to 45 m of diameter), slaloms (cones at distances between 25 and 40 m), chicanes and turns with variable radius.

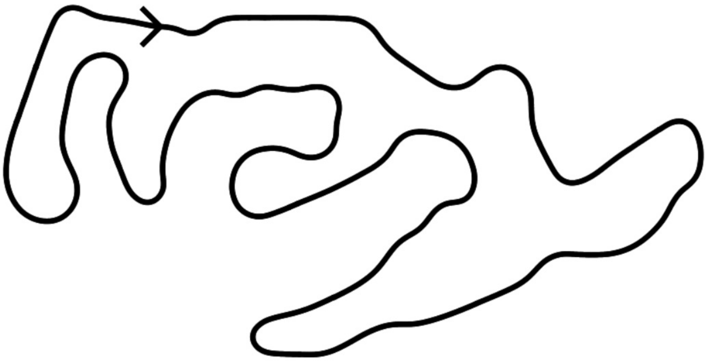

Figure 1.3: *FSAE Germany Autocross track (2012).*

Endurance and fuel economy

The endurance is the event that ends the race weekend and aims at evaluating the overall performance of the prototype. For this reason it represents the main event of a Formula

SAE competition. It takes place along a track very similar to the one in which the autocross test is run, for a total of 22 km. Team members are not allowed to intervene on the vehicle while the test is underway, while a change of driver is expected in the middle of the test, during a three-minute rest period. The starting order is decided on the autocross results. The overall time of the endurance is given by the sum of the times of each driver plus the eventual penalties; the score depends on the total time compared to the fastest team. During the endurance also the fuel economy is evaluated: no refuelling is allowed and points are given based on consumed averaging litres of fuel per kilometer.

1.3 The Race UP Team

The University of Padova has participated at the Formula Student events since 2006 with the Race UP team. The team, composed of about thirty students from different faculties, is divided in seven departments:

1. Aerodynamics
2. Frame & Body
3. Suspensions
4. Brake
5. Electronics
6. Engine & Drivetrain
7. Business & Marketing

Every department has to design different parts of the car following the guidelines decided at the beginning of the season. In 2015 has been created also the electric division which has the goal to design and build an electric car to compete in the formula electric events.

- II -

Car Aerodynamics

The aerodynamic development for competition cars has started in the 1910s. At the beginning the main focus of these studies was the attempt to reduce drag using elongated shapes that delayed the separation of the flow. The first car designed with a wing system, in order to generate downforce, is the Chaparral 2e of 1966; from that moment different manufacturers tried to maximize the aerodynamic development to increase the performance, not only in terms of drag reduction, but also to seek greater vertical load that would allow the car to have better characteristics of drivability and stability. Currently the aerodynamic development, according to the type of car and championship, is strictly regulated in order to guarantee a certain level of safety.

Figure 2.1: *Chaparral 2e (1966)*

2.1 Aerodynamic forces

Aerodynamic forces can be divided into two categories:

1. pressure forces, which act normal to the surfaces;
2. shear forces, which act parallel to the surfaces.

The resultant from these forces can be divided into various components; the most common directions are defined by a coordinate system based on the car three reference axes. The three components are:

1. drag, along x axis, that is the direction of the car movement;
2. lift, along z axis;
3. side forces along y axis.

These three force components can be represented by non-dimensional coefficient defined as:

$$D = \frac{1}{2} C_D A \rho V_\infty^2 \tag{2.1}$$

$$L = \frac{1}{2} C_L A \rho V_\infty^2 \tag{2.2}$$

$$Y = \frac{1}{2} C_Y A \rho V_\infty^2 \tag{2.3}$$

As it is possible to see, the aerodynamic forces depend in particular on a certain area of reference, but especially they are proportional to the square of the speed. For the performance of a car the two most important components are drag and lift; as concern the side forces, these are important in the case of side winds and overtaking, where the stability of the car can be compromised.

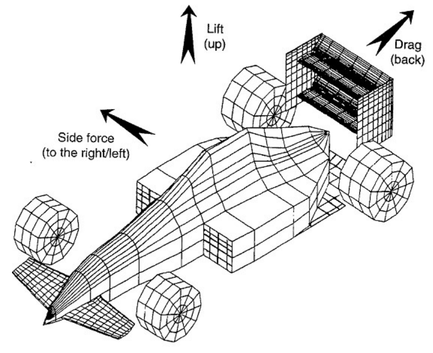

Figure 2.2: *Aerodynamic forces [2]*

2.1.1 DRAG

The overall drag of the car is considered as the resistance to the vehicle motion; in addition to the fluid-dynamic effect, the component due to the rolling wheels must be considered. In particular, this resistance assumes a value comparable to the aerodynamic drag for low speeds, while it results to be much lower at higher speeds. Another important aspect that influences the total drag of the car is due to the detachment of the flow from the surface of the car. This can happen essentially for two reasons: for the geometry of the car and for the positive pressure gradient that can cause the detachment of the flow. The first case is illustrated in Figure2.3: a net cut of the geometry causes a zone of flow recirculation, creating a low pressure region that increases the aerodynamic resistance effect. In order to understand the second case, it is necessary to explain the behaviour of the fluid near the wall.

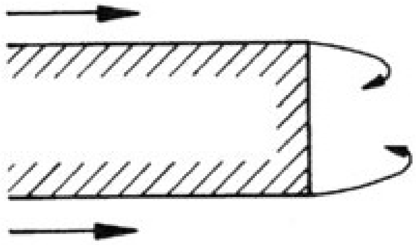

Figure 2.3: *Example of flow detachment caused by body shape [3]*

Boundary Layer

At the interface between fluid and wall, the velocity of the fluid, due to its viscosity, is zero: this condition is known as no-slip condition. The velocity increases moving away from the wall until it reaches the undisturbed condition, creating a velocity gradient which develops within a certain distance from the surface: this layer is called the boundary layer. The exact thickness of the boundary layer can not be defined due to its asymptotic pattern; it is then established as the distance from the surface at which the fluid has a velocity equal to 99% of the undisturbed flow. The thickness of the boundary layer grows along the surface, in particular the speed with which it increases depends on:

- inertia and friction forces (Reynolds number);
- evolution of static pressure along the surface.

The boundary layer is sensitive to pressure variation; in particular, if the increase in pressure is too steep, it can cause the detachment of the flow from the surface. This behaviour is easily visible considering a two-dimensional example. The pressure along a body follows the trend as in Figure2.4; the kinetic energy of the fluid is entirely converted into pressure at the stagnation point and from that point up to the thickest part of the body the flow is accelerated, the static pressure decreases and the kinetic energy of the fluid increases. Within the boundary layer due to the dissipative effects of friction, part of the kinetic energy is dissipated. Beyond the thickest point of the body, the pressure starts to rise, reducing the kinetic energy and causing a change in the velocity profile, within the boundary layer, due to the slowing down of the particles in contact with the surface. At the point where the kinetic energy is completely converted into pressure, the inversion of the velocity profile takes place and this involves the detachment of the flow from the surface (Figure2.5).

At the beginning, the boundary layer is generally laminar, but as the thickness increases, it arrives at a transition zone that brings the boundary layer to be turbulent (Figure2.6); generally, for low values of Reynolds number, the boundary layer is laminar, but there is a zone in which both the laminar and turbulent conditions can exist and this will depend only on the boundary conditions. In case of turbulent boundary layer the thickness is higher (Figure2.7) because of the flow fluctuations inside it; furthermore, a laminar boundary layer generally generates a lower resistance due to a lower friction coefficient. However, the turbulence transfers momentum in the normal direction to the surface, for this reason, the turbulent boundary layer tends to detach later than the laminar layer; in particular this condition is sought in the rear part of the car and on particularly

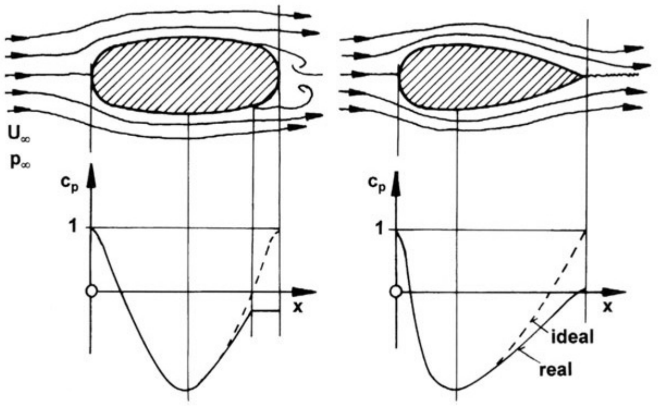

Figure 2.4: *Trend of cp and velocity along a body [3]*

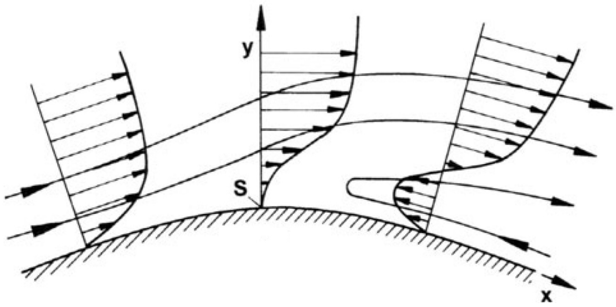

Figure 2.5: *Velocity profile inside the boundary layer [3]*

loaded wings, where a slight increase in drag is preferred to avoid separations that would significantly damage the performance.

2.1.2 LIFT

As defined above, the lift is the force in the direction perpendicular to the body motion. To explain briefly where this force derives from it is useful to consider a two-dimensional aerodynamic profile invested by a fluid. Because of its shape and its angle of attack the flow will have different pressure and speed above and below the profile; in particular in the case of Figure2.8 there will be higher pressure on the upper side (pressure side) and lower pressure on the lower side (suction side). This difference generates a resulting upward force called lift. Using Bernoulli's law it is possible to establish a correlation between speed and pressure along a streamline:

$$\frac{p}{\rho}\frac{V^2}{2} = const \qquad 2.4$$

This means that along the suction side, where the pressure is lower, there will be an higher velocity, while, on the other hand, at the pressure side the flow will be slower.

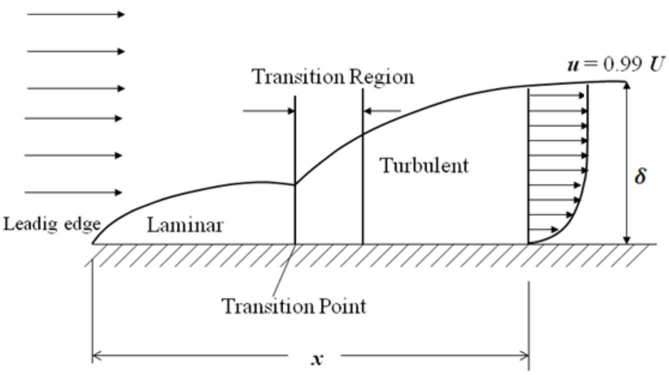

Figure 2.6: *Boundary Layer transition*

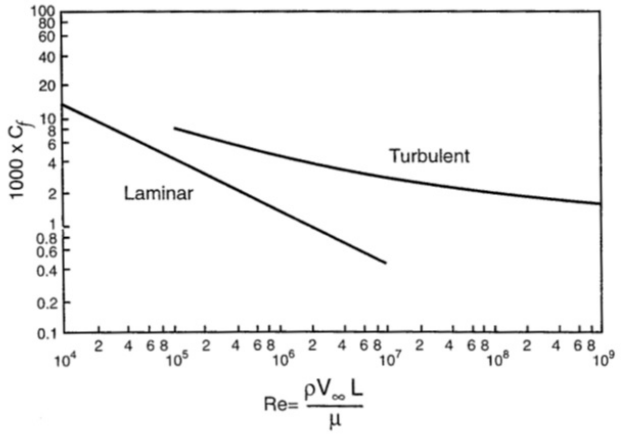

Figure 2.7: *Relation between friction coefficient and Re [2]*

2.2 Forces effect

As already said above, the aerodynamic forces are exploited in the automotive field to improve the performance. A car touches the ground only through the four points determined by the contact patch between the road and the tyres; through these areas all the forces, necessaries for the motion of the car, are transmitted to the ground as frictional forces. The frictional forces are proportional to the area and to the normal force at the surface, so, simply increasing the load on the wheels, the car is able to transmit more force to the ground. Through the aerodynamic forces it is possible to increase the load on the wheels without increasing the weight of the car: this allows, for example, to raise the speed during the turning phase because if the load on the wheels is higher also the frictional force of the tires will be greater and therefore the adhesion of the car will be improved. On the other hand, drag creates resistance to the motion of the car limiting the performance especially in terms of maximum speed. The creation of downforce automatically generates an increase in drag: this implies the research of a compromise that depends on different aspects such as car type, track and external conditions. To generate aerodynamic load,

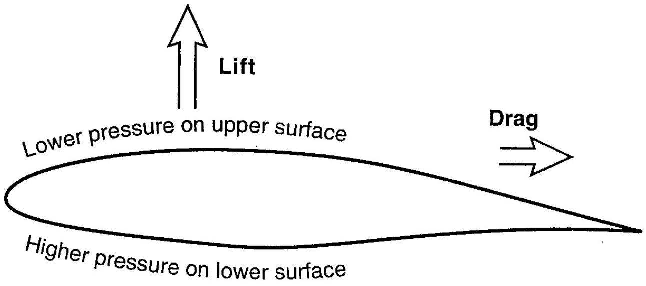
Lift
Drag
Lower pressure on upper surface
Higher pressure on lower surface

Figure 2.8: *Airfoil[2]*

different strategies can be used:

1. Change the shape of the car using spoiler, airdam or splitter;
2. Use wings;
3. Exploit the shape of the car.

The first strategy is used especially for closed-wheels cars where the use of wings is less common for various reasons. The purpose of these appendages is usually to create a downward force by exploiting an increase of the static pressure and a reduction of the speed.

2.2.1 WINGS

The use of wings allows to create an high vertical load, but as already explained above, this also involves the creation of drag. These are some important parameters for the geometry of the airfoil:

Leading edge: this is the most advanced point of the airfoil;

Trailing edge: it is the most backward point of the airfoil;

Chord: line that joins the leading edge to the trailing edge;

Pressure side: side of the airfoil characterized by an increase in static pressure;

Suction side: side of the airfoil characterized by an increase in speed;

Camber line: line that joins equidistant points between pressure side and suction side;

Half-thickness: distance between the middle line and the sides;

Angle of attack: angle between the chord and the direction of the undisturbed speed;

Span: extension of the wing in the direction perpendicular to the section of the airfoil;

Aspect Ratio: ratio between span and chord.

All these parameters, besides defining the shape of the airfoil, influence its performance. The optimal shape of the profile may change depending on the operating conditions of the wing; for example, in the presence of ground effect, a profile with a lower thickness will have better performance exploiting the interaction with the ground better than a thicker airfoil. The behaviour of a profile is strongly influenced by its angle of attack. The Cl has a trend that is directly proportional to the angle of attack until the stall condition is reached; the stall occurs at high angles of attack where the pressure gradient is so steep that it causes the flow detachment and a sharp drop of the Cl value. The Cd, instead, has a rising trend with the angle of attack, so the adjustment of the wing inclination requires a compromise between downforce and drag.

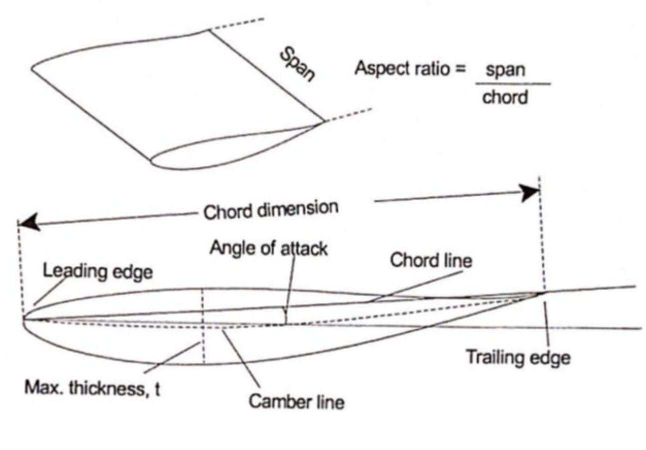

Figure 2.9: *Airfoil*

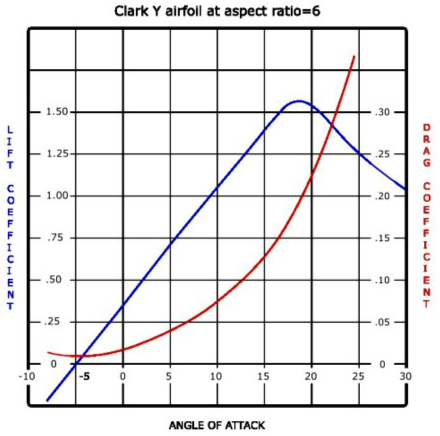

Figure 2.10: *Cl and Cd*

The aspect ratio gives an indication on the development of the wing in the two main directions. In particular, a high aspect ratio ensures better performance because the edge effects, due to the finished span of the wing, are limited to a lower portion of the surface. If we consider a three-dimensional wing of finite extension, at the edges the flow at higher pressure (pressure side) will try to move towards the lower pressure area (suction side) causing the reduction of the global downforce. For this reason lateral plates (end plates or side fins) are used to limit this phenomena by maintaining the pressure difference between the two sides of the wing; their effect can be seen as an increase of the aspect ratio of the wing described by the following relation [2]:

$$AR = AR_{fin}\left(1 + 1.9\frac{h}{b}\right) \tag{2.5}$$

where AR_{fin} is the aspect ratio of the finite wing, h is the endplate height and b is the wing span.

A multi-element configuration can be used to increase the downforce produced by the wing. In this set-up, at least one other airfoil is added to the main wing (mainplane), it is usually smaller than the main and it is called flap. The addition of the flap creates a series of phenomena that increase the performance of the wing; first, the global wing surface rises and even the overall camber of the wing grows ensuring an increase in the downforce. Furthermore, the flap has the effect of diverting the flux more to the trailing edge of the main, increasing the overall angle of attack; the flow velocity increases on both the main surfaces and in particular on the trailing edge, where this reduces the negative effects of the adverse pressure gradient and therefore delays the separation of the boundary layer. The combination of these effects generates a growth of the global downforce. Additional elements are generally placed behind the mainplane, but it is possible to place a small wing in front of it, called *slat*. The slat is usually the smallest element of the wing and it is characterized by a negative angle of attack; its role is different from the flaps because it is used to avoid the separation at the leading edge that can affect highly cambered wings. The most important parameters for the design of a multi element wing are the relative dimensions of the elements and the gap between them; general rules for their definition have been defined based on experimental tests. To increase the downforce produced by the rear wing a common solution is using a gurney (or wickers). The gurney is a small strip ($\approx$ 10/15 mm) attached to the trailing edge of the rearmost element of the wing, usually perpendicular to the surface. It has the effect of adding a vertical component to the velocity at the trailing edge: this has a similar effect to adding more camber to the wing. It also increases the static pressure above the wing and produces two counter rotating vortices that help to keep the flow attached. Therefore, despite a small extra drag, the gurney flap increases the downforce produced.

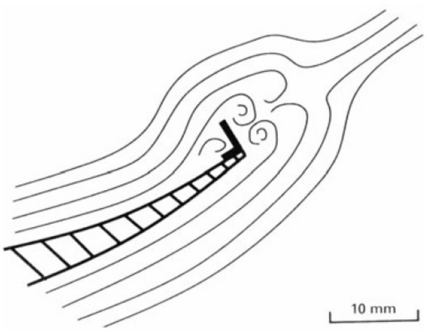

Figure 2.11: *Gurney flap [4]*

2.2.2 UNDERTRAY

The last way to create vertical aerodynamic load is by exploiting the shape of the vehicle and in particular the underbody airflow. The simple idea behind this strategy is to create a clean airflow under the car, using also the ground effect, in order to accelerate the air and thus reducing the static pressure; this causes a net vertical load without increasing the drag. The easiest solution is to use a flat underbody surface, but to improve the performance "intake" systems and diffuser are used to create a Venturi tunnel effect. The diffuser angle is very important because it influences the static pressure recovery and if it is too steep it can causes the detachment of the flow. Furthermore the diffuser co-operate with the rear wing and, from experimental test, has been seen that if the rear wing is near enough to the diffuser it can help to keep the flow attached and to extract the air from the underbody. Another relevant variable is the distance from the ground; due to the ground effect the force produced increases as the height of the car is reduced until it reaches a critical distance where the flow is blocked from going under the car (this happens when the distance is similar to the boundary layer thickness).

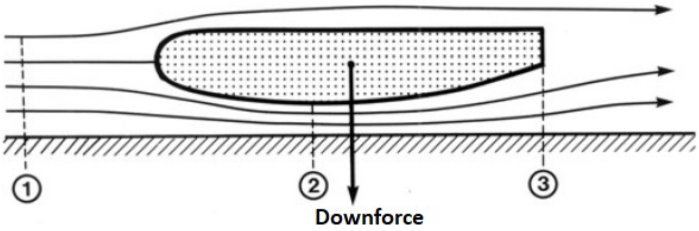

Figure 2.12: *Underbody working principle [4]*

- III -

CFD

Computational Fluid Dynamics, or CFD, is the analysis of systems involving fluid flow, heat transfer and associated phenomena such as chemical reactions by means of computer-based simulation [8]. The main advantage of the CFD is that it provides fast and cost-effective results for fluid dynamic problems in a reasonable amount of time.

3.1 MATHEMATICAL MODEL

At the base of the CFD there is a system based on these three equations:

- Conservation of mass;
- Conservation of momentum;
- Conservation of energy.

These three lead to the Navier-Stokes's equation:

$$\rho \frac{Du}{Dt} = -\frac{\partial p}{\partial x} + div(\mu\, grad\, u) + S_X \tag{3.1}$$

$$\rho \frac{Dv}{Dt} = -\frac{\partial p}{\partial y} + div(\mu\, grad\, v) + S_Y \tag{3.2}$$

$$\rho \frac{Dw}{Dt} = -\frac{\partial p}{\partial z} + div(\mu\, grad\, w) + S_Z \tag{3.3}$$

Depending on the characteristics of the problem and of the flow the system can be simplified. In particular it is very important to define the type of the flow analysed because it can change drastically the mathematical problem. The main characteristics which have to be defined are the following:

- Incompressible/Compressible;
- Steady-state/Transient;
- Laminar/Turbulent;
- Inviscid/Viscous;

- Sub- /Transonic;
- Single- /Multiphase.

For the solution of fluid dynamic problems there are three different methods, which are all under the CFD group:

- Finite difference method;
- Finite element method;
- Finite volume method.

In our case we consider the finite volume method, which is the most used by commercial software. In this method the entire domain is divided in small volumes, where the system of equations is evaluated at the centroid of each cell. Generally, the finite volume method can be resumed in the following steps:

1. Decomposition of the problem domain into control volumes;
2. Formulation of integral balance equations for each control volume;
3. Approximation of integrals by numerical integration;
4. Approximation of function values and derivatives by interpolation with nodal values;
5. Assembling and solution of discrete algebraic system.

3.2 The process

The simulation process can be divided into three phases:

- Pre-processing
- Solver
- Post-processing

3.2.1 Pre-processing

The pre-processing phase consists in the setting of all the input for the resolution of the CFD problem.

Geometry

The first step is the definition of the geometry. In most cases the geometry must be imported from an external CAD software using one of the universal format such as .iges or .step. The preparation of the geometry is one of the most important and time consuming step for the CFD. Normally the CAD file of the object is very detailed and it contains every components, but, for the CFD, it is necessary to simplify the geometry deleting all the parts that do not affect the flow behaviour; this allows to create a better mesh using less elements which means a more robust and faster resolution of the problem. The CFD software solve the fluid domain, for this reason a boolean operation, which subtracts the geometry from a bigger domain, must be compute. The domain must be large enough to let the flow freely evolve during the simulation. For example in order to simulate a car, it is defined a prismatic domain, similar to a box, which contains the car; as a rule of thumb, this "box" must extend five times the length of the object in the front direction, in the lateral direction and in the vertical direction, while for the rear it should extend for ten times to consider all the wake phenomena. Lastly the car is subtracted from the box obtaining the final domain. The computational time necessary to the resolution depends also on the dimension of the domain, for this reason if the geometry is symmetric, respect to the flow conditions, it is possible to reduce the domain exploiting this property.

Mesh

The domain has to be divided into small volumes, or cell. The solution to a flow problem (velocity, pressure, temperature etc.) is defined at the centroid node inside each cell. The accuracy of a CFD solution is governed by the number of cells in the grid. Generally if the number of cells is higher the solution accuracy will be better, but this requires more time for the resolution and also more computational power. However in some case a too finest mesh can bring to instability problem and the solution can diverge. The mesh elements can be of different shape; in 3D the most used elements are:

- Tetrahedral cell shape;
- Hexahedral cell shape;
- Prismatic cell shape;
- Polyhedral cell shape.

The best shape depends especially on the geometry of the object; the tetrahedric mesh allows to reproduce complex geometries, but it is more time-consuming to solve, while the hexahedric mesh is better for the computational time required, but it is less suitable for complex geometries. The polyhedric mesh is a trade-off between the two above-mentioned. The prismatic elements are used near the surface to reproduce the boundary layer. It is also possible to combine different types of mesh to exploit the quality of each shape. Optimal meshes are often non-uniform: finer in areas where large variations occur from point to point and coarser in regions with relatively little change; to do this CFD software provide the possibility to use mesh refinement defined by the user or by the software automatically. The mesh refinement can be on both the element size and the cell growth rate.

To evaluate the mesh quality there are different parameters (Figure 3.4) to check:

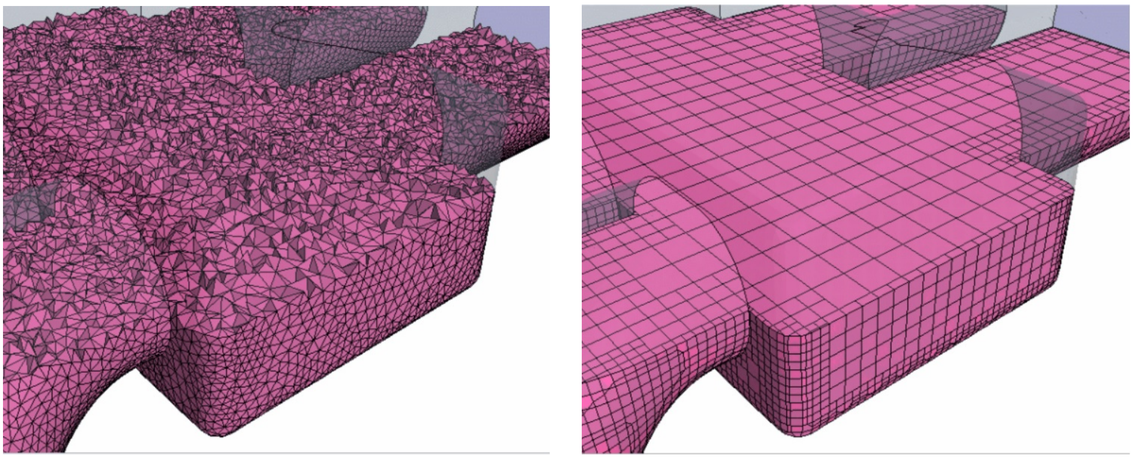

(a) *Tetrahedral mesh* **(b)** *Hexahedral mesh*

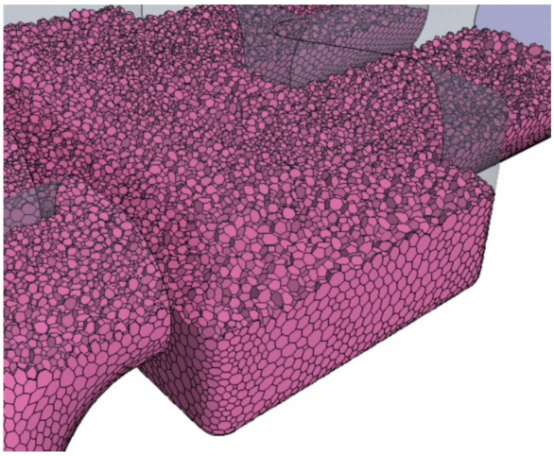

(c) *Polyhedral mesh*

Figure 3.1: *Different types of element shape [5]*

- Skewness angle;
- Cell aspect ratio;
- Volume change;

The skewness angle is the angle between the face area vector (face normal) and the vector connecting the two cell centroids; an angle of zero indicates a perfectly orthogonal mesh. Problems result because the diffusion term formulation for transported scalar variables contains the dot product in the denominator, and this dot product is zero when the angle is 90 degrees. Cell aspect ratio defines the ratio between the cell sizes in different dimensions; a cell with an aspect ratio of one is considered perfect. Volume change describes the ratio of the volume of a cell to that of its largest neighbour; a large jump in volume from one cell to another can cause potential inaccuracies and instability in the solvers.

Definition of the physical phenomena

The next step in the pre-processing phase is defining the physical problem to analyse. As reported above, there are different characteristics that define the fluid behaviour. The

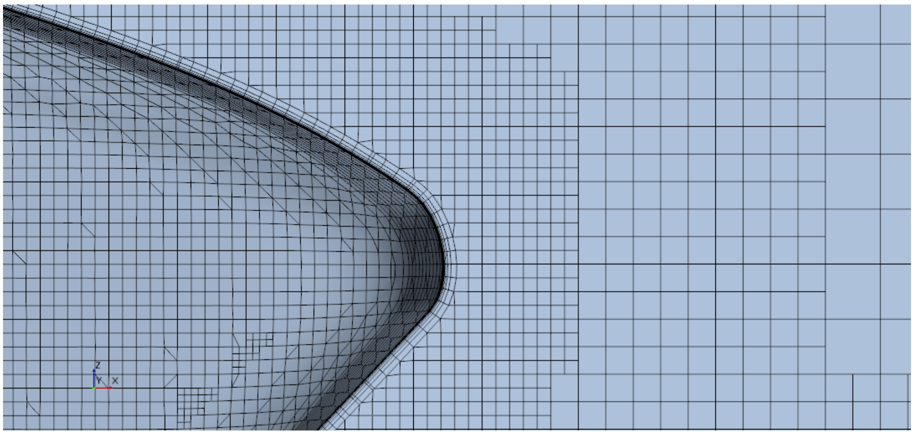

Figure 3.2: *Prismatic mesh for the boundary layer*

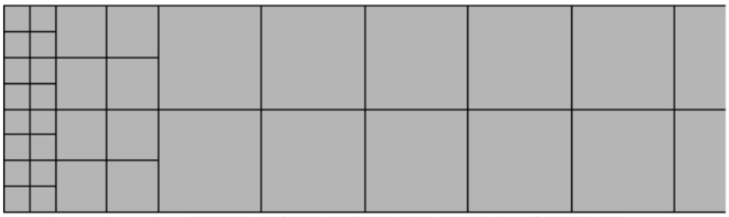

Medium Growth Rate (2 Layers per Cell Size)

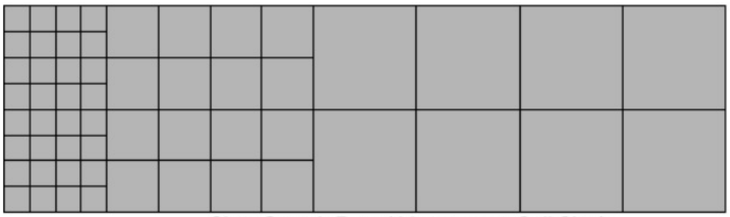

Slow Growth Rate (4 Layers per Cell Size)

Figure 3.3: *Cell growth rate [5]*

first aspect to define is the fluid compressibility. Incompressible flow means that the fluid density is constant and this occurs for mostly all liquids and for low speed gas flow (normally under Ma<0.3); in this case the equations system is simplified because there is one less variable and so the energy equation can be neglected. Instead, for compressible flow the density is a variable of the system and then also the energy equation must be solved; gases at speed over 0.3 Ma are considered compressible.

After the definition of the fluid compressibility, the analysis type must be chosen. The behaviour of the fluid can be time-dependent and in this case it is denoted as transient flow; for example the body wake and the relative vortex can be considered as a transient phenomena. On the other hand if the flow does not exhibit time dependant behaviour it will be a steady flow. An important parameter for a fluid dynamic problem is the Reynolds number; this is defined as the ratio between the inertial and the viscous forces:

$$Re = \frac{\rho u L}{\mu} \tag{3.4}$$

where ρ is the flow density, u is the velocity of the flow with respect to the object, L is the characteristic length and μ is the dynamic viscosity. The Reynolds number (Re) is

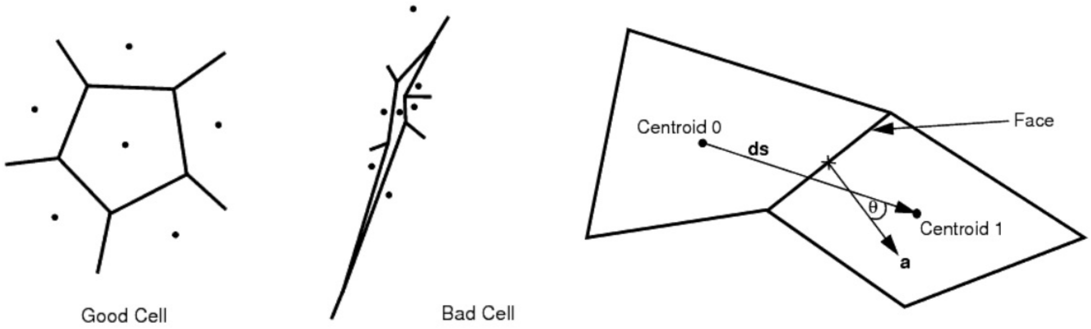

(a) *Aspect ratio* **(b)** *Skewness Angle*

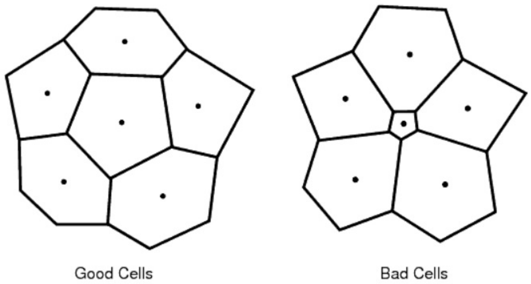

(c) *Volume change*

Figure 3.4: *Different types of mesh quality index [5]*

a non-dimensional number that describes the flow turbulence; for high values of the *Re* the flow becomes turbulent. The critical value depends on the geometry and on the fluid properties: for example, for a flow in a pipe the critical *Re* is 2300. Turbulent conditions means a chaotic and random state of motion in which the velocity and pressure change continuously with time within substantial regions of flow; this leads to an intrinsically unsteadiness even with constant boundary conditions. Turbulence is characterized by the presence of eddies, vortices and vortex stretching which are extremely dissipative processes. If the *Re* is below the critical value the flow is considered laminar, it is smooth and adjacent layers of fluid slide past each other in an orderly fashion; in this case if constant boundary conditions are applied the flow is steady. To simulate this kind of phenomena in CFD

Compressible	**Incompressible**
- Constant density - Mass and Momentum conservation only - No Energy balance - Mostly all Liquids - Low speed gases (Ma<0.3)	- Variable density - Mass and Momentum conservation - Energy balance solved - High speed gases (Ma>0.3)

Table 3.1: *Difference between compressible and incompressible*

turbulence models have been developed. The two most used models for RANS simulation are the k-ϵ and the k-ω. Both these methods add two more variables, and two more equations, to the mathematical system:

- Turbulent kinetic energy (k);
- Turbulent dissipation (ϵ or ω).

The right model depends on the flow condition and on the geometry. K-ϵ works very well for external flow cases without flow separation, but it performs poorly for rotating flows and for flow characterised by adverse pressure gradients and flow separation, predicting excessive levels of turbulence. On the other hand, the k-ω model performs very well near the surfaces and it has poor performance in the free stream region. For this reason it has been created an hybrid model, the k-ω SST, that combines the k-ϵ in the cells far from the wall with the k-ω model for the cells near the surfaces. The k-ω SST is suitable for external flow analysis with flow separation, such as the simulation of an airfoil; the main disadvantage is that it is computationally more expensive than the other two standard methods and it requires a very accurate mesh to converge. It has already been discussed the behaviour of the flow near walls in chapter 2: for the non slip condition the flow has velocity equal to zero at the wall and it creates a region, called boundary layer, where it recovers the free stream velocity according to a velocity profile. The boundary layer can be laminar or turbulent; the laminar boundary is a very smooth flow, while the turbulent boundary layer contains swirls or eddies. Laminar flow creates less skin friction drag than turbulent flow, but is less stable. Boundary layer flow over a wing surface begins as a smooth laminar flow. At some distance back from the leading edge, the smooth laminar flow breaks down and transitions to a turbulent flow. The behaviour of the turbulent boundary layer is different from the free stream due to the presence of the wall. It is possible to identify three different regions inside the boundary layer:

- Viscous sublayer
- Buffer layer
- Log-law region

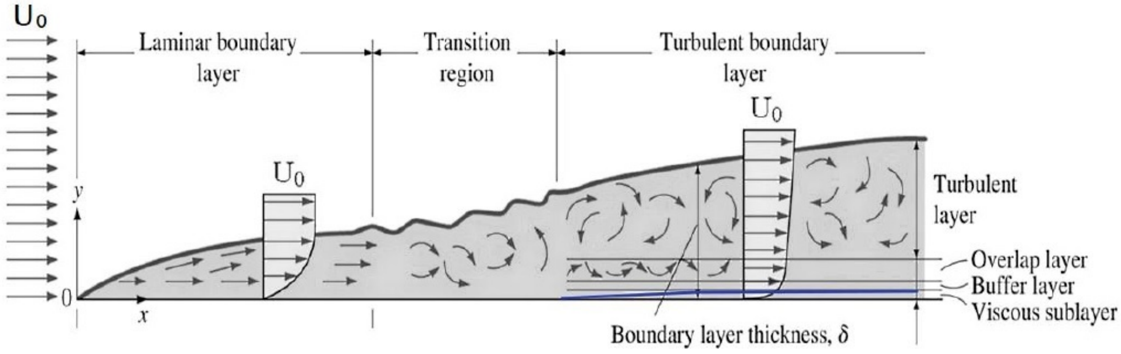

Figure 3.5: *Boundary Layer development [6]*

In order to describe the flow inside the boundary layer is helpful to define these three parameters:

$$Wall\,shear\,stress \qquad \tau_w = \mu \left(\frac{\partial u}{\partial y} \right)_{y=0} \tag{3.5}$$

$$Friction\,velocity \qquad u_* = \sqrt{\frac{\tau_w}{\rho}} \tag{3.6}$$

$$Non-dimensional\,wall\,distance \qquad y^+ = \frac{u_* y}{\nu} \tag{3.7}$$

$$Law\,of\,the\,wall \qquad u^+ = \frac{U}{u_*} = f(y^+) \tag{3.8}$$

Where

u^+ is the non-dimensional velocity;

U is the flow velocity;

ρ is the fluid density;

y is the distance form the wall.

In the region known as the viscous sublayer, below 5 wall units, the variation of u+ to y+ is approximately 1:1, such that:

$$y^+ = u^+ \tag{3.9}$$

Because of this relationship it is also known as the linear sub-layer. Outside the viscous sublayer ($30 < y^+ < 500$)exists a region where viscous and turbulent effects are both important; in this region the law of the wall, also called log-law, can be written as:

$$u^+ = \frac{1}{k} \ln y^+ + C^+ \tag{3.10}$$

where

k is the Von Kàrman constant;

C^+ is a constant.

In the buffer layer, between 5 wall units and 30 wall units, neither the log-law or the linear relationship holds, such that:

$$u^+ \neq y^+ \tag{3.11}$$

$$u^+ \neq \frac{1}{k} \ln y^+ + C^+ \tag{3.12}$$

with the largest variation from either law occurring approximately where the two equations intercept at y^+=11; before 11 wall units the linear approximation is more accurate and after 11 wall units the logarithmic approximation should be used. It is possible to plot the behaviour just described using a logarithmic diagram obtaining the Figure3.6.

In CFD the y^+ is defined by the height of the first cell of the boundary layer. To solve the boundary layer completely it is necessary to keep the y^+ value under 5, or better

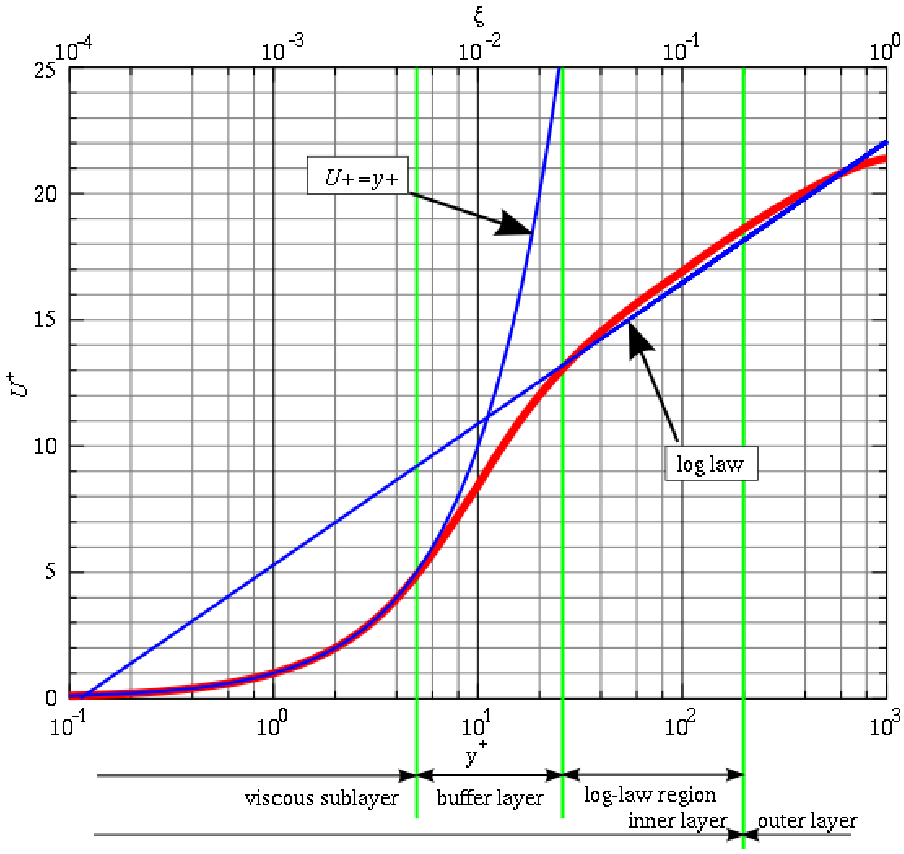

Figure 3.6: *Law of the wall [7]*

under 1; however this brings to very large and computationally expensive mesh. In order to reduce the number of cells, it is possible to use wall functions that mathematically approximate the turbulent profile for log-law region (y^+>30), but they can be used only in case of no flow separation.

To define completely the physical phenomena of the problem it is necessary to set the fluid phase: if the simulation regards only a single fluid this will be a single phase flow; on the other hand if there are two or more different fluids or different phases (for example air-water, oil-water) this will be a multiphase flow. Single phase is obviously easier than multiphase which is more time consuming and requires also the interface tracking of the different phases.

Boundary conditions

The last step for the pre-process is defining the boundary conditions of the problem. There are three different types of boundary conditions:

- the Dirichlet condition: sets a fixed value for a flow variable at the boundary considered;
- the Neumann condition: sets a fixed derivative value for a flow variable at the boundary considered;
- the mixed condition: combination of the previous.

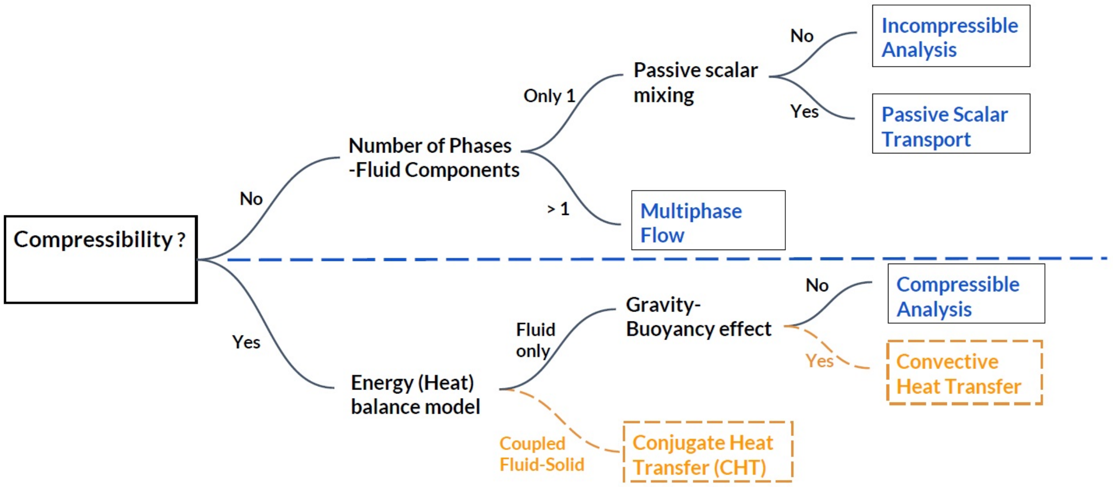
Compressibility ?
No
Yes
Number of Phases
-Fluid Components
Only 1
> 1
Passive scalar
mixing
No
Yes
Incompressible
Analysis
Passive Scalar
Transport
Multiphase
Flow
Energy (Heat)
balance model
Fluid
only
Coupled
Fluid-Solid
Gravity-
Buoyancy effect
No
Yes
Compressible
Analysis
Convective
Heat Transfer
Conjugate Heat
Transfer (CHT)

Figure 3.7: *CFD physical phenomena summary*

The boundary conditions must be defined in order to admit only one feasible solution. For example consider a 2D analysis of an airfoil, if the boundary conditions set the total pressure and the total temperature at the inlet and the total pressure at the outlet, this will lead to infinite solutions in case of isentropic flow; while if the condition at the outlet regards the static pressure, this allows only one feasible solution. The right conditions depend on the physics of the problem and there is no unique possibility. In external aerodynamic the most commonly used boundary conditions are the following:

- Velocity inlet
- Total pressure inlet
- Symmetry
- Pressure outlet

3.2.2 Solver

There are different numerical solution techinques for CFD problem; as it has already been discussed it is possible to defined three distinct streams of numerical solution methods: finite differences, finite elements and finite volumes. The physical phenomena considered in the CFD are complex and non-linear so an iterative approach and a numerical scheme for the resolution are required. The numerical schemes can be classified on the order of interpolation, that is linked to the order of the derivatives considered, and on the direction of the interpolation. The most used numerical schemes are the following:

- First order upwind
- Central differencing scheme
- Second order upwind

To solve the equations system is possible to use different algorithm; the most popular procedures are:

- TDMA (tri-diagonal matrix algorithm)
- SIMPLE
- Gauss Seidel
- Conjugate Gradient
- Multi-Grid method

3.2.3 POST-PROCESSING

The post-processing phase is necessary to understand if the results obtained from the analysis can be reliable. CFD software provide the possibility to create scenes showing the distribution of scalar or vector quantities; using these images is possible to understand the behaviour of the flow around the body. The forces and moments can be directly calculated by the software as an integral of the pressure over the surfaces considered.

Convergence criteria

CFD software use an iterative algorithm to the resolution of the fluid domain; for this reason monitoring the residuals is very important. To reach the convergence the residuals must satisfy two main aspects:

- max value: the max value among all the residuals must be below a certain value that depends on the physics of the problem and on the definition of the residuals;
- constant trend: the residuals value must be stable, without fluctuation.

In addition to this, it is very useful to check the trend of relevant scalars, for example in case of wing simulation drag and lift are the most common scalars used. If the scalar stays around a steady value this is a sign of reached convergence. Various observations can be done studying the residuals and the scalars; in particular if a steady state analysis is performed and the residuals or the scalars are periodically oscillating probably the problem is intrinsically unsteady.

- IV -

EXPERIMENTAL TEST

Experimental tests were performed on the MG X.15 car of the University of Padova, as a topic of a master thesis [9]. The MG X.15 was the first car of the Race UP team with a complete aeropack; in particular it was equipped with a three elements front wing, a four-element rear wing and aerodynamic sidepods. The main goal of the experimental tests was to measure the aerodynamic forces of the rear wing.

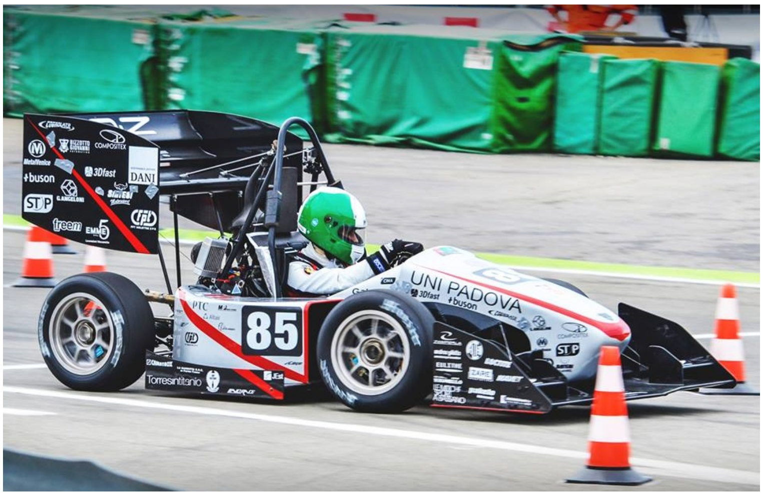

Figure 4.1: *MG X.15*

4.1 SENSORS SET-UP

The rear wing of the MG X.15 was attached to the chassis by six tubular supports (Figure4.2.

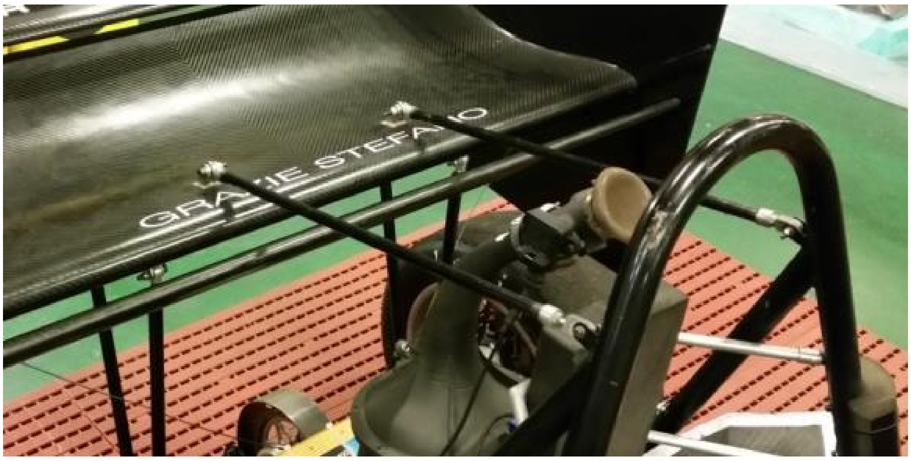

Figure 4.2: *Rear wing attachment system*

The original tubes were made of carbon fibre with aluminium inserts at the extremities to attach the rod-end. In order to measure the loads produced by the wing was decided to use six home made load cells, one for each tube; to obtain better results the original tubes were replaced by aluminium ones, which have a behaviour easier to predict and measure. The load cell was made of a circular section tube, attached to the supports by M6 screws; two strain gauges were placed on two opposite sides of the circle, as it is possible to see from the Figure4.3.

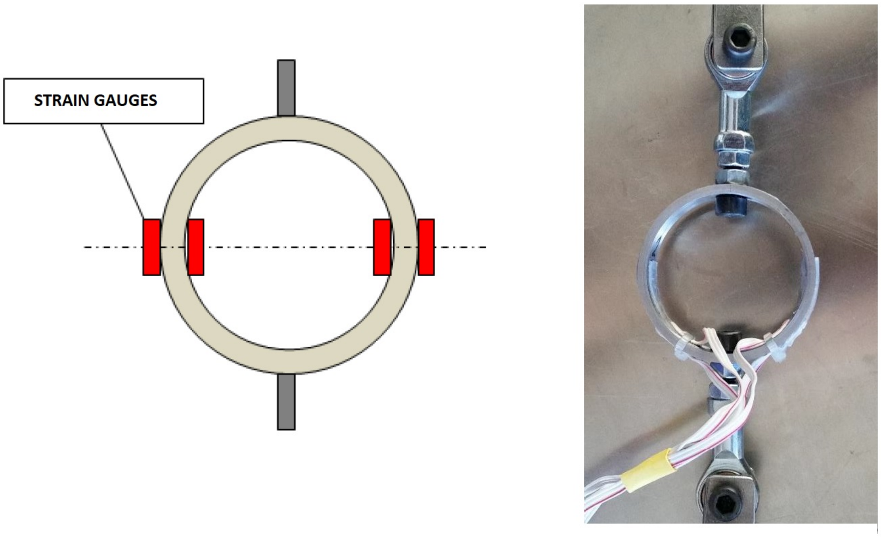

Figure 4.3: *Load cell*

The load cells were calibrated and then placed on the car and connected by wirings to a control unit that stored all the data measured during the test. The final set-up was the one represented in Figure4.4.

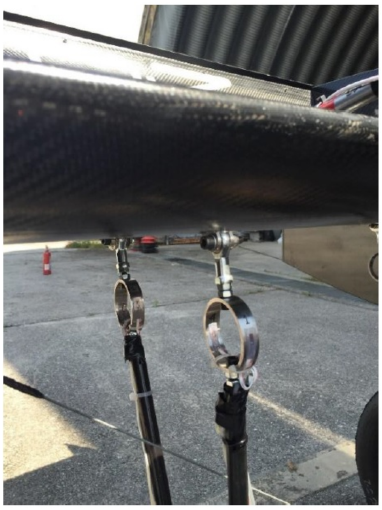

Figure 4.4: *Final set-up*

4.2 THE TEST

Various tests were performed, but the one that is considered in this thesis is the constant velocity run. In the constant velocity test the car was driven at an established speed along a straight line in both ways, so that the wind effects could be evaluated from the loads measured. The test was performed at four different speed:

- Run at 30 km/h
- Run at 50 km/h
- Run at 70 km/h
- Run at 90 km/h

The speeds chosen are the most significant velocity for a FSAE car. To obtain better results the temperature of the air, the atmospheric pressure and the velocity of the wind were measured before every run; from the temperature and the pressure also the air density was deduced, so that more precise values for lift and drag coefficients could be obtained. Three different rear wing set-up were tested (Figure4.6):

- Acceleration set-up (Low load)
- Medium load configuration
- High load configuration

The three configuration differ in flaps angle of attack and relative position of the wing elements. The airfoils were fixed to the endplates by four M3 screws, two per each side; different holes in the endplates were used to change the aerodynamic configuration. Before each run, relative distances and angles between the elements (Figure4.5) were measured so that it has been possible to reproduce the exact disposition of the profiles using a CAD software.

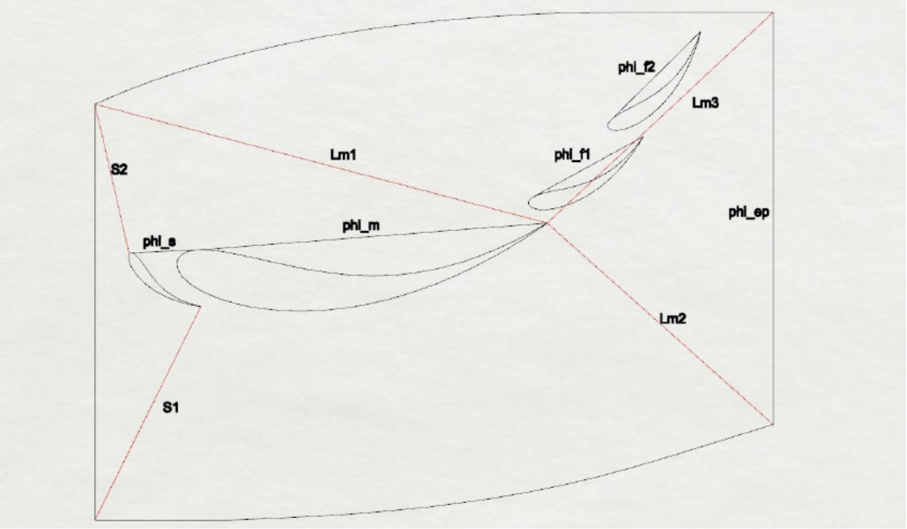

Figure 4.5: *Relative distance and angles*

	DX	SX	
Lm1	525 mm	525 mm	
Lm2	340 mm	340 mm	
Lm3	348 mm	345 mm	
S1	261 mm	260 mm	
S2	167 mm	169 mm	
Phi_s	-1.9°	-1°	
Phi_m	4.3°	4.2°	
	HIGH	MEDIUM	ACCELERATION
Phi_f1	5.1 mm	25.5 mm	31.3 mm
Phi_f2	17.9 mm	46.5 mm	56.4 mm
L_f1_3	214 mm	200 mm	195 mm
L_f2_3	83 mm	87 mm	108 mm

Table 4.1: *Relative distances and angles*

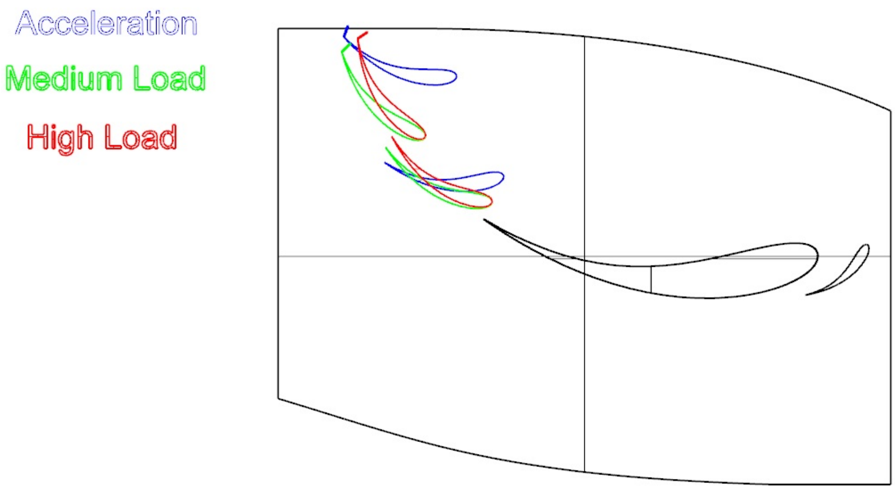

Figure 4.6: *Configurations tested*

4.3 Data analysis

The load cells on the supports measure the load on the direction of the tube, but, in order to evaluate the aerodynamic effect, the forces were decomposed into the two main axis x and y according to the scheme 4.7.

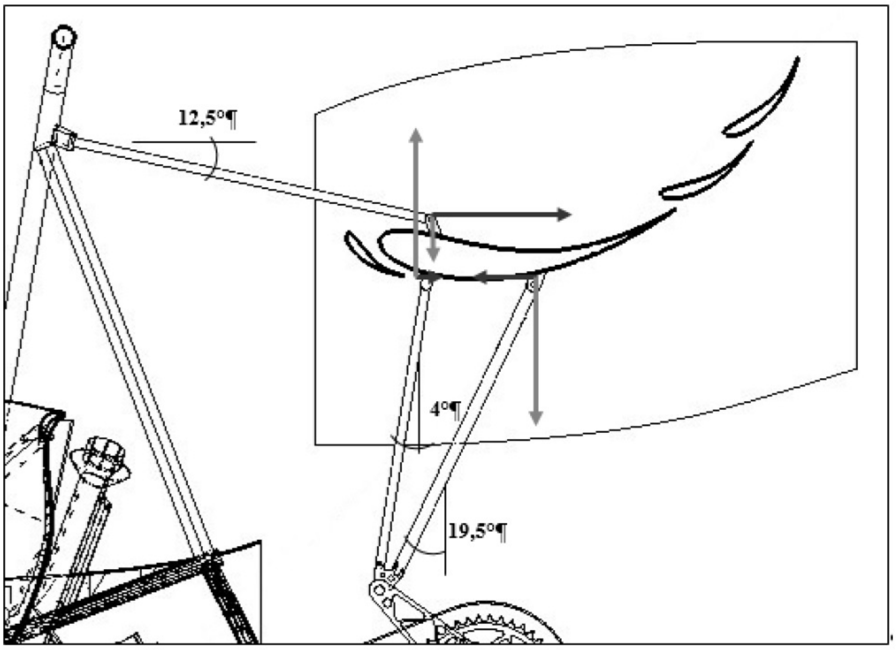

Figure 4.7: *Angles for the decomposition*

From the acquisition system (Figure4.8) was possible to monitor the car speed and the load cells output signal.

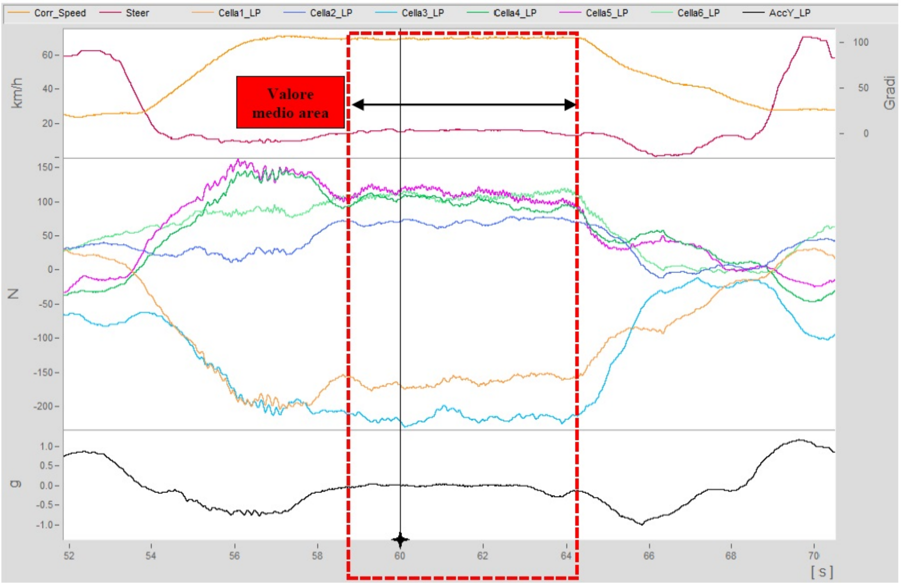

Figure 4.8: *Example of acquisition output*

The total force was averaged on an interval time at constant speed; from this a value of $C_l * A$ and $C_d * A$ were deduced as follows:

$$C_l * A = \frac{Lift}{\frac{1}{2}\rho V^2} \tag{4.1}$$

$$C_d * A = \frac{Drag}{\frac{1}{2}\rho V^2} \tag{4.2}$$

This procedure was done for both the run at the same speed; the results were often different due to the wind effect. An important hypothesis was made on the wind velocity: as a matter of fact the wind speed and direction were considered equal between the two run so that in one case it was an advantage for the aerodynamic performance and a disadvantage in the other run. An average aerodynamic coefficient was calculated from the two runs and using this was possible to obtain the effective speed of the air relative to the wing.

$$V_{run} = \left(\sqrt{\frac{L_{run}}{\frac{1}{2}\rho C_{l_{ave}} A}}\right) \tag{4.3}$$

The results are the following:

Speed (km/h)	Density (kg/m3)	Avg DF (N)	Avg Drag (N)	Wheel Speed (km/h)	Correct speed (km/h)	Correct Cl*A	Correct Cd*A
30	1.1964	44.73	12.75	31.6	34.31	0.823	0.235
30	1.1964	30.41	5.79	31.1	28.29	0.823	0.157
50	1.1964	67.92	24.09	51.6	53.51	0.514	0.182
50	1.1964	63.13	23.04	53	51.3	0.519	0.189
70	1.1964	109.87	45.322	68.75	73.14	0.445	0.183
70	1.1964	84.19	35.98	68.71	64.02	0.445	0.190
90	1.1964	198.27	74.33	91.35	97.83	0.449	0.168
90	1.1964	159.5	61.56	95	87.75	0.449	0.173

Table 4.2: *Acceleration set-up*

Speed (km/h)	Density (kg/m3)	Avg DF (N)	Avg Drag (N)	Wheel Speed (km/h)	Correct speed (km/h)	Correct Cl*A	Correct Cd*A
30	1.1914	40.093	15.696	31	31.65	0.870	0.340
30	1.1914	36.827	14.032	31.1	30.33	0.870	0.331
50	1.1914	127.062	48.444	50.62	59.62	0.777	0.296
50	1.1914	57.987	21.465	51.46	40.28	0.777	0.287
70	1.1914	237.874	100.553	69.91	80.31	0.806	0.339
70	1.1914	126.8	54.35	70.93	58.51	0.805	0.345
90	1.1914	378.6	166.25	89.4	103	0.776	0.341
90	1.1914	185.91	86.22	87.9	72.2	0.776	0.359

Table 4.3: *Medium load configuration*

Speed (km/h)	Density (kg/m3)	Avg DF (N)	Avg Drag (N)	Wheel Speed (km/h)	Correct speed (km/h)	Correct Cl*A	Correct Cd*A
30	1.1922	80.224	36.782	30.5	38	1.208	0.554
30	1.1922	21.799	73.209	29.5	19.8	1.209	0.400
50	1.1922	139.54	58.14	50.87	57.1	0.931	0.388
50	1.1922	82.88	31.47	51	44	0.931	0.354
70	1.1922	231.62	101.698	70.9	74.1	0.917	0.402
70	1.1922	186.65	80.73	69.8	66.5	0.918	0.397
90	1.1922	367.1	159.45	89.37	95	0.884	0.384
90	1.1922	271.84	119.86	87.5	81.7	0.885	0.390

Table 4.4: *High load configuration*

The results show as the Cl and Cd are very different for the tests performed at 30 km/h, this is due to the greater influence of the wind at low velocity; for this reason to calculate the final values of the aerodynamic coefficient the results at 30 km/h were neglected. To complete the data analysis the results at different speed were averaged and to consider measurement errors also the standard deviation was evaluated. Therefore the final Cl and Cd for the three configuration are:

Configuration		Cl*A	Cd*A
Acceleration set-up			
	Average	0.470	0.181
	Standard deviation	0.033	0.008
	Max value	0.503	0.189
	Min value	0.437	0.173
Medium Load			
	Average	0.786	0.328
	Standard deviation	0.014	0.013
	Max value	0.800	0.341
	Min value	0.773	0.315
High load			
	Average	0.911	0.386
	Standard deviation	0.019	0.001
	Max value	0.930	0.387
	Min value	0.892	0.385

Table 4.5: *Final results*

These values for the aerodynamic coefficients have been used for the validation of the CFD model of the MG X.15.

- V -

VALIDATION

In order to perform reliable fluid dynamic analysis, the CFD model must be validate comparing the results obtained with experimental data. The goal is to create a mesh model based on the MG X.15 geometry and validate it using the results obtained from the Chapter4. The software used for the CFD simulation is STAR CCM+, which was provided by the CD-Adapco to the University FSAE team. To design the CAD geometry of the car both Creo Parametric 3.0 and Rhinoceros have been used. The geometry and the meshing strategy were changed to improve the results of the CFD simulation in order to obtain values of $Cl * A$ and $Cd * A$ similar to the experimental ones; in this chapter the starting point simulation and the following most representative attempts will be described.

5.1 SIMULATION SET-UP

The simulation performed was a second order RANS 3D steady analysis using the $k\omega SST$ turbulence model. Moreover, since the analysed flow was air at low speed, the fluid was defined as incompressible and single-phase. Exploiting the car symmetry, only half of the car was studied, in this way it was possible to reduce significantly the cells number. To discretize the domain an hexahedric mesh was used, with a prismatic structure to reproduce the boundary layer near the surface; for the boundary layer was used a particular set-up called *"All y+ wall treatment"* that combines the complete resolution if the y+<5 and the wall functions if the y+>30. The aerodynamic set-up used for the validation process was the medium load configuration at a speed of 50 km/h (13.889 m/s). The dimension of the domain was chosen using general guidelines for car aerodynamic (Figure5.1) described in Chapter **??**. The boundary conditions used are the following:

- Inlet: velocity inlet, $V_0 = 13.889 m/s$;
- Outlet: pressure outlet at atmospheric pressure;
- Symmetry and Far: symmetry condition;
- Ground: moving wall at $V = 13.889 m/s$ with no-slip condition.

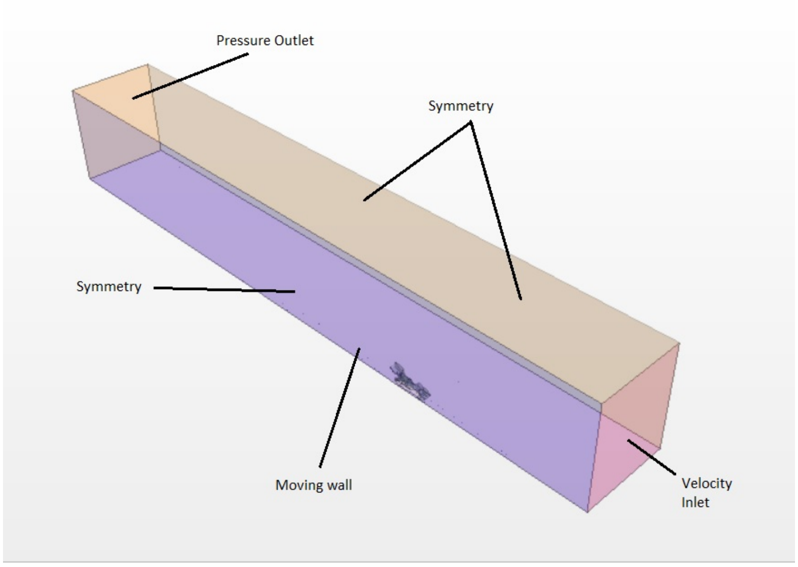

(a) *Boundary conditions*

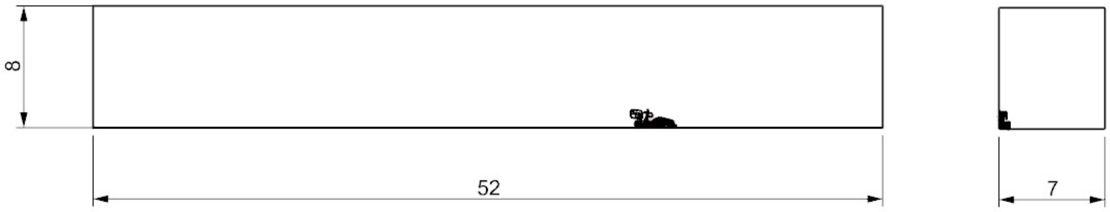

(b) *Domain dimensions*

Figure 5.1: *CFD domain*

For all the relaxation factors and numerical parameters the default values were maintained.

5.2 GEOMETRY PREPARATION

The MG X.15 was designed using Creo Parametric; the complete CAD of the car is very detailed because the position of every single components must be verified before the manufacture phase. However, for the CFD analysis, many parts of the vehicle were negligible and they only added useless geometry complexities. Starting from the original CAD the geometry was simplified using Rhinoceros following these general guidelines:

Car body: the body of the car was transformed in a closed cell that reproduces the external geometry of the vehicle;

Driver: obviously the driver was not present in the CAD file, but it is very important for the CFD analysis: for this reason a dummy driver was added;

Engine: the engine is one of the most complex parts of the car; it was simplified using simple geometric bodies that follows the general shape of the engine block;

Wheels: the wheels were replaced with filled cylinder to avoid the internal flow inside the rims;

Suspension system: the dampers and the bell cranks were deleted, while the wishbones were preserved;

Transmission system: the transmission system was simplified using closed geometry;

Front wing, Rear wing and Sidepods: these are the only geometries that must not change from the original CAD;

Chassis: only the rear tubes were reproduced in the CFD geometry because the front part of the chassis was covered by the car body;

Radiator: the radiator was replaced by a parallelepiped oriented with the same inclination of the original geometry and defined as a porous media.

5.3 Starting geometry

During the design phase of the MG X.15 a CFD CAD was realised to perform the fluid dynamic analysis. Observing the two images Figure5.2 and Figure5.3, which show the CFD and the original CAD, it is possible to notice the simplifications described above. The idea was to use this simplified model as a starting point, trying to improve the geometry and creating a reliable and validated mesh model.

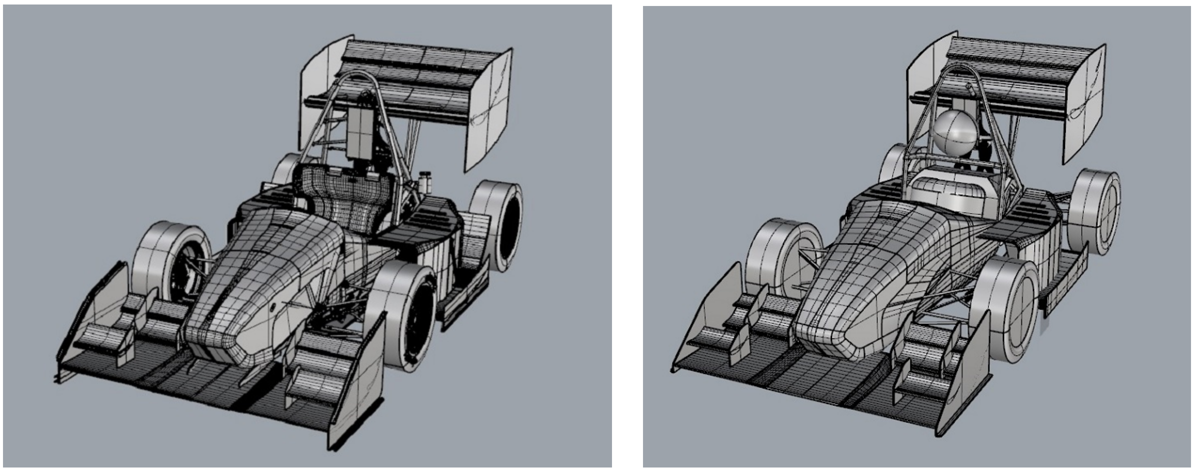

(a) *Original CAD* **(b)** *CFD CAD*

Figure 5.2: *Original CAD and CFD CAD*

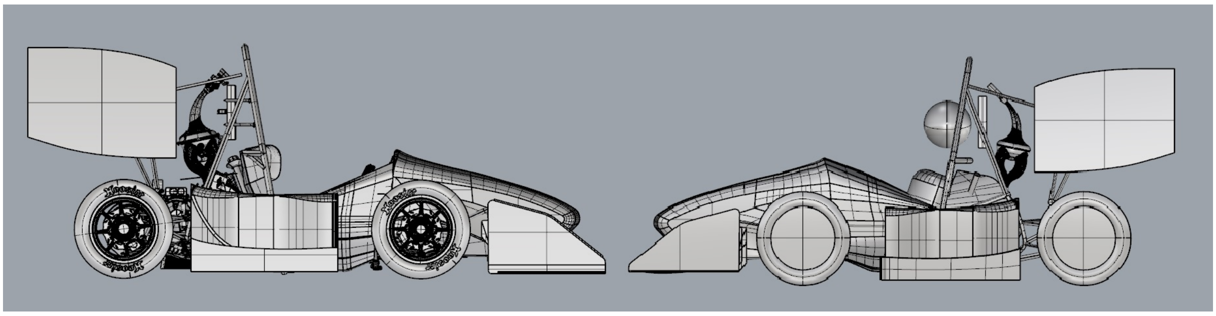

Figure 5.3: *Original CAD and CFD CAD*

The mesh used was a non-structural hexahedric mesh combined with a prismatic structure for the boundary layer. To improve the model quality different mesh refinements were used; the main characteristics and refinements are listed in Table5.1.

Base size	90 mm
Target surface size	38 mm
Minimum surface size	3.1 mm
Number of prism layers	18
Prism layer near wall thickness	0.01 mm

Refinements	
	Volumetric control
	Car volume
	Line control
	Wings trailing edge
	Surface control
	Boundary surfaces
	Wings
	Wake refinement
	Whishbones

Table 5.1: *Refinements used*

The result was a 10.7 mln elements mesh (Figure5.4). Observing the Figure5.4, it is possible to notice that the wake area was not well refined and this may cause problems in the results because the wake region is characterized by high level of turbulence and therefore it shall be discretized with finer elements; this was due to the low computational power available at that time. Moreover the geometry in the rear part of the car was different from the real vehicle, in particular, the engine block was too small and was not linked to the transmission system.

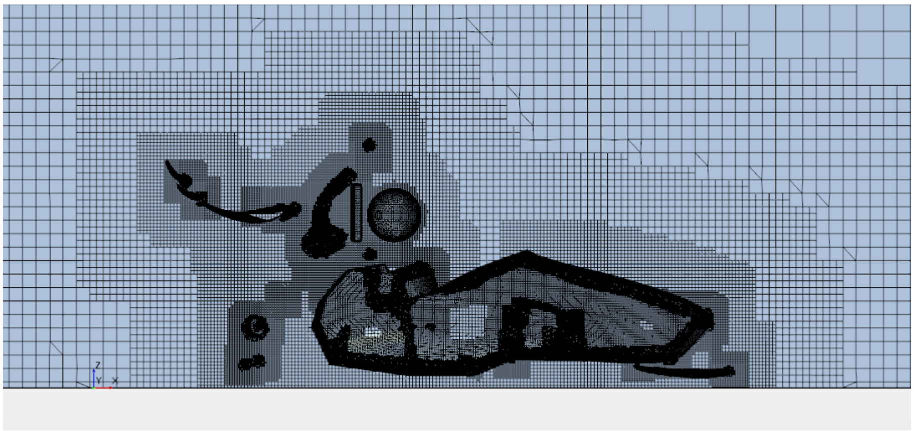

Figure 5.4: *Original mesh*

After 9000 iterations the simulation was stopped, as it reached forces convergence; the final results in terms of $Cl * A$ and $Cd * A$ for the rear wing are the following:

	Cl*A	Cd*A	Cl*A error (%)	Cd*A error(%)
Experimental test	0.7865	0.328		
Original mesh	0.896	0.333	13.95	-2.33

Table 5.2: *Original mesh results*

The errors obtained are not bad, especially for the C_d value, but the geometry of this first CAD model was too simplified to obtain trustworthy values.

5.4 First Attempt

In order to achieve more reliable results the geometry was modified and in particular these elements were added:

- a block to reproduce the engine;
- a simplified geometry of the transmission which rotates around its axis;
- a more realistic airbox and driver model.

The main problem for the previous mesh was the computational power available for the simulation: this involved a maximum number of cells that was too low to describe in a proper way all the domain. First was generated a mesh reducing the base size (from 90 mm to 75 mm): in Star ccm+ the base size is similar to a unit of measurement of the mesh and it is possible to define all the refinements and all the controls respect to this value. In order to improve the $y+$ value on the rear wing the trailing edge of the profiles were squared and a curve control was defined for them. The number of the mesh elements increased from 10.7 mln to 17.5 mln (Figure5.7).

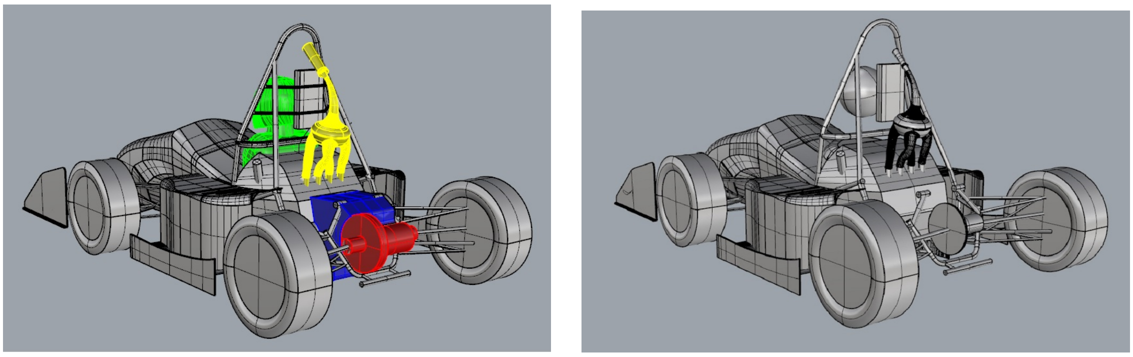

(a) *Modified CAD* **(b)** *First attempt CAD*

Figure 5.5: *Modified elements*

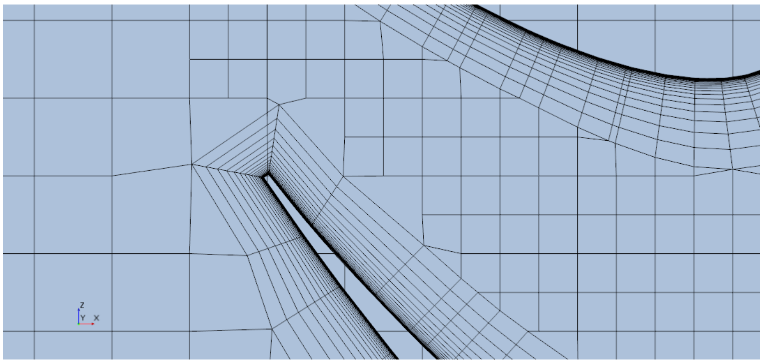

Figure 5.6: *Squared trailing edge*

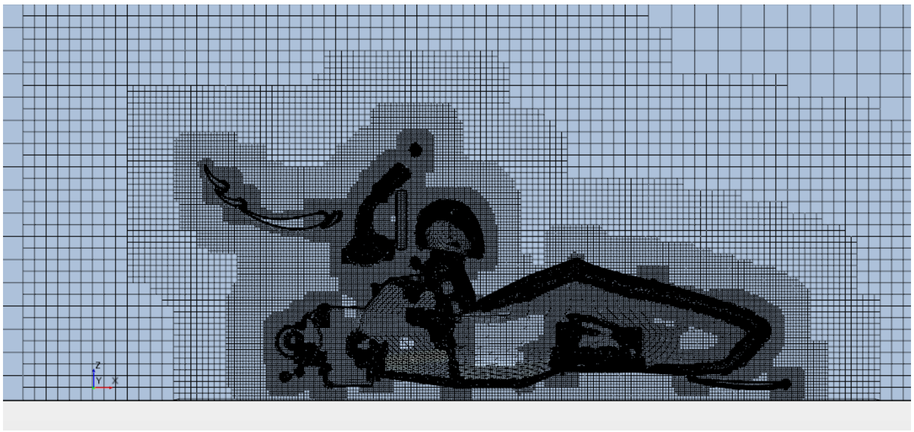

Figure 5.7: *First attempt mesh*

The simulation was stopped after 25000 iterations to verify the trend of the residuals and the forces; the results are the following:

	Cl*A	Cd*A	Cl*A error (%)	Cd*A error(%)
Experimental test	0.7865	0.328		
Original mesh	0.896	0.333	13.95	-2.33
First Attempt	1.048	0.387	33.22	13.51

The first thing that is possible to notice is that the error became larger compared to the original simulation, but, for the reason described above, the previous model cannot be considered reliable. The value of the $y+$ on the rear wing (Figure5.8) were improved on the trailing edge, but few elements were still above the limit ($y+ < 5$); this happened because near the attachment lines of the wings to the end-plate the boundary layer structure was not formed.

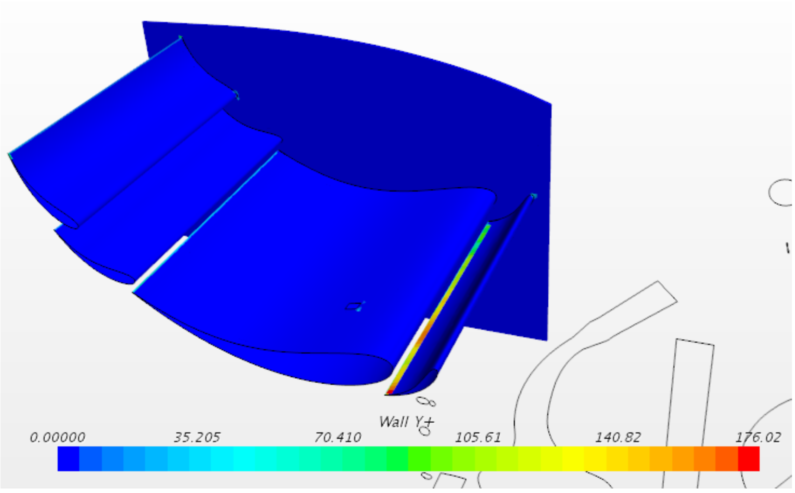

(a) *Starting point* $y+$

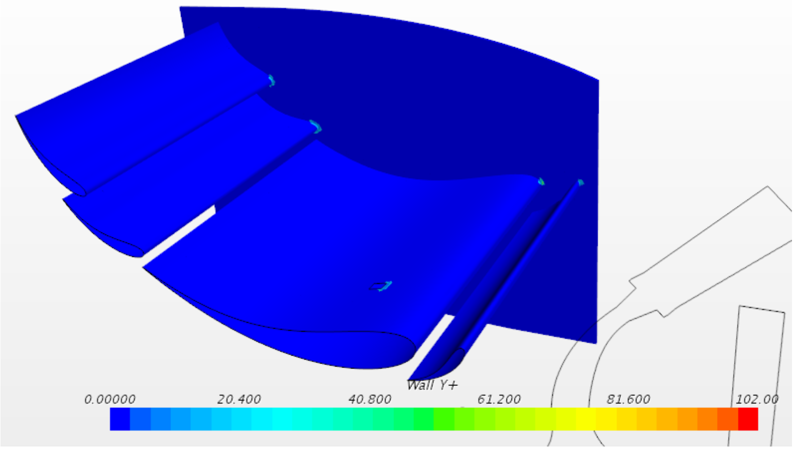

(b) *First attempt* $y+$

Figure 5.8: $y+$ *distribution on the rear wing*

5.5 SECOND ATTEMPT

In order to realize a complete discretization of the boundary layer, the parameters of the *"prism layer mesher"* were changed: in particular the *"minimum thickness percentage"*, which retracts the cell layers to zero when the total thickness is under its value, was reduced from 20 to 12.5. The controls on the boundary layer are global and thus they affect all the domain; for this reason the mesh base size was increased (from 75 mm to 130 mm) in order to contain the mesh dimension. The result was a 17.4 mln elements mesh (Figure5.9).

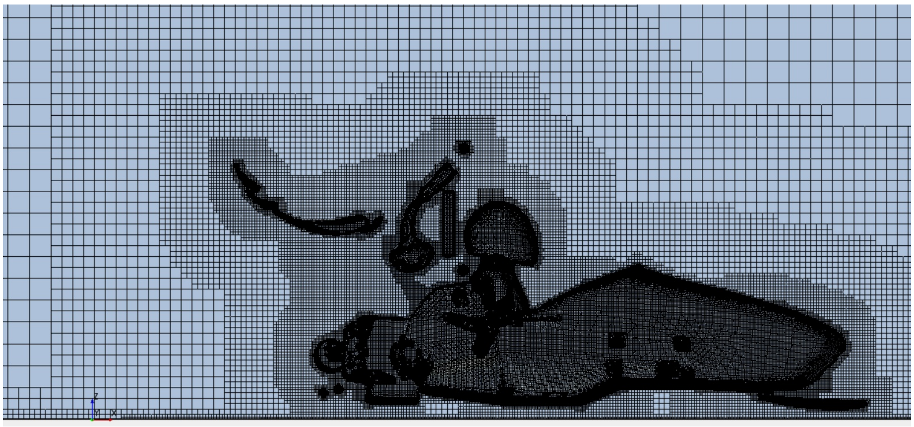

Figure 5.9: *First attempt mesh*

After the resolution the $y+$ values on the rear wing were analysed: the reduction of the *"minimum thickness percentage"* allowed to model completely the boundary layer on the wings keeping all the cells under the limit (Figure5.10). Nevertheless the aerodynamic coefficients did not change from the previous attempt.

	Cl*A	Cd*A	Cl*A error (%)	Cd*A error(%)
Experimental test	0.7865	0.328		
Original mesh	0.896	0.333	13.95	-2.33
First Attempt	1.048	0.387	33.22	13.51
Second Attempt ($y+$ improvement)	1.039	0.374	32.05	9.81

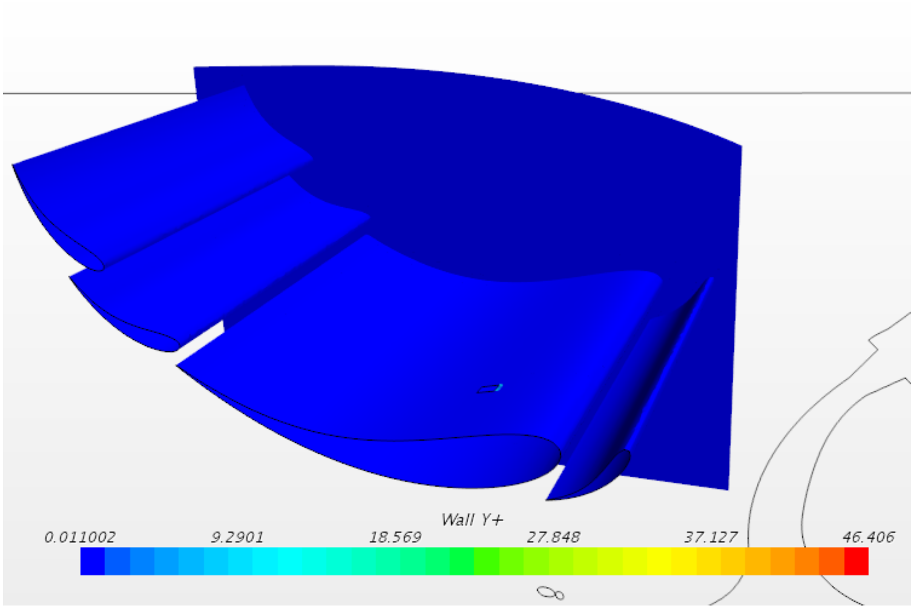

Figure 5.10: *Second attempt rear wing y+*

Another aspect, which is visible plotting the velocity field on the symmetry plane (Figure5.11), is that the rear wake of the car was not well defined because of too larger elements in that area. Furthermore the residuals (Figure5.12) reached a steady value after 4000 iterations, but the asymptotic value remained too high (≈ 5E-02).

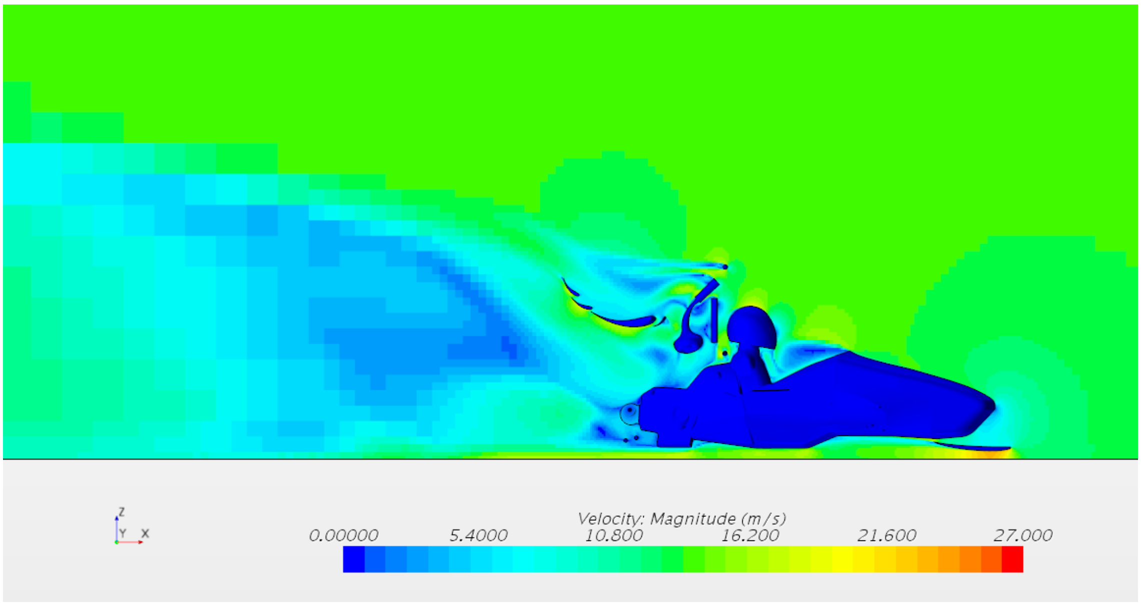

Figure 5.11: *Second attempt velocity scalar field*

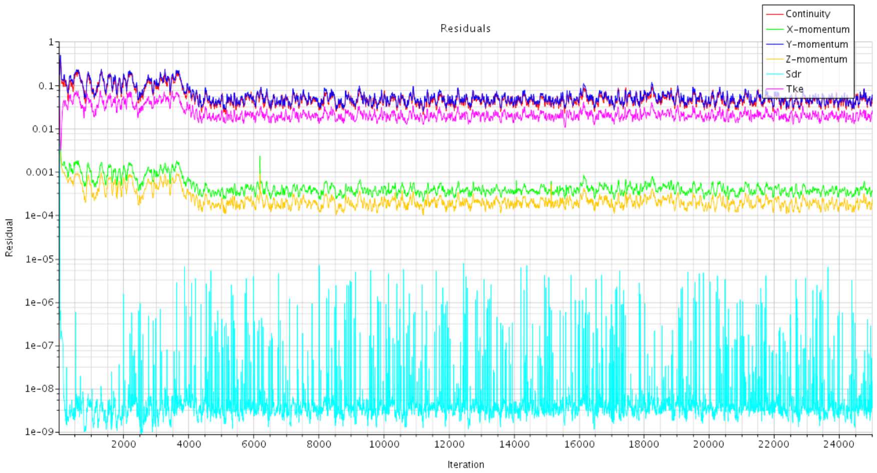

Figure 5.12: *Second attempt residuals*

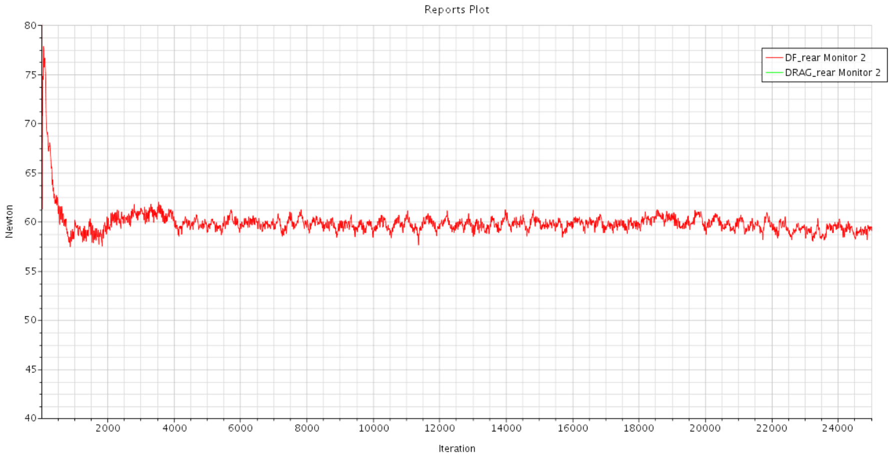

Figure 5.13: *Second attempt downforce*

5.6 THIRD ATTEMPT

For the third attempt the focus was on trying to improve the mesh quality using different refinements in sensitive areas. First a curve control was defined for all the trailing and leading edge of the wings to obtain smaller elements and thus reproduce more precisely the profiles. Surface controls were applied to all the cylindrical components (wishbones, chassis, rear wing supports and transmission) to create smoother surfaces. Moreover Star ccm+ gives the possibility to set a refinement on the wake of an established surface, setting the spread angle and the length of the wake: this control is called $wake\ refinement$. In this attempt the $wake\ refinement$ was used for the wheels, the rear wing, the car body and the transmission system. The resulting mesh counted 24.4 mln elements (Figure5.14) and, compared to the previous, it was improved especially on the wake region, using smaller elements for the discretization.

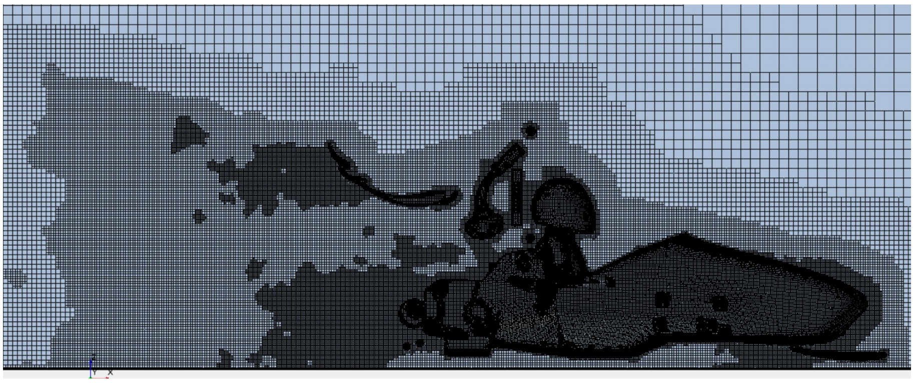

Figure 5.14: *Third attempt mesh with wake refinement*

From the previous case it was observed that the residuals and the forces reached a steady value after 4000 iterations, therefore this simulation was stopped after 8000 iterations.

	Cl*A	Cd*A	Cl*A error (%)	Cd*A error(%)
Experimental test	0.7865	0.328		
Original mesh	0.896	0.333	13.95	-2.33
First Attempt	1.048	0.387	33.22	13.51
Second Attempt ($y+$ improvement)	1.039	0.374	32.05	9.81
Third Attempt (wake refinement)	1.004	0.359	27.68	5.35

The $Cl * A$ and $Cd * A$ slightly improved, but they were still far from the experimental results. However the wake area compared to the previous attempt reproduced better the velocity scalar field (Figure5.15).

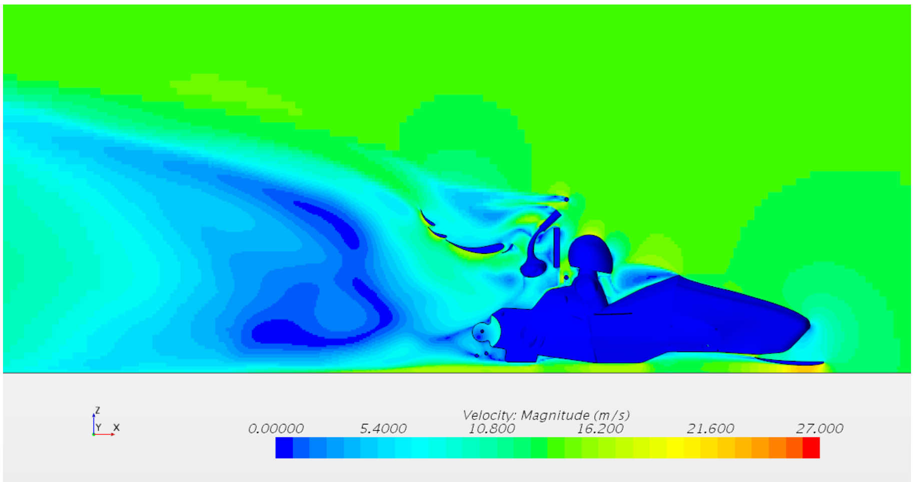

Figure 5.15: *Third attempt velocity scalar field*

5.7 Fourth Attempt

At the first time some details were neglected in order to start from a simpler geometry; at this point the gurney flap (Figure5.16) was added at the rear wing on the rearmost flap. The gurney used for the experimental test was an aluminium strip of 15mm height, fixed at the trailing edge by six M3 screws.

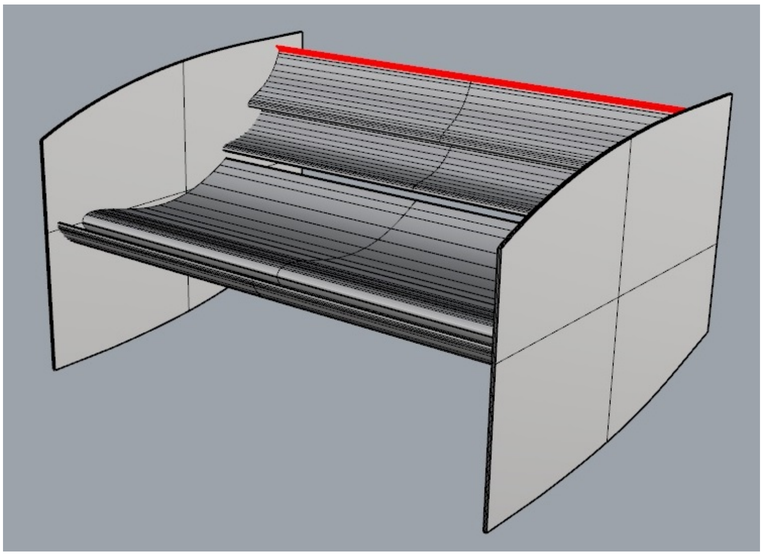

Figure 5.16: *Rear wing with gurney*

The mesh set-up was not changed and so also the mesh dimension was almost the same (24.7 mln).

	Cl*A	Cd*A	Cl*A error (%)	Cd*A error(%)
Experimental test	0.7865	0.328		
Original mesh	0.896	0.333	13.95	-2.33
First Attempt	1.048	0.387	33.22	13.51
Second Attempt (y+ improvement)	1.039	0.374	32.05	9.81
Third Attempt (wake refinement)	1.004	0.359	27.68	5.35
Fourth Attempt (gurney)	1.079	0.400	37.2	17.3

As expected the $Cl * A$ and $Cd * A$ increased both, due to the effect of the gurney.

From Figure5.17 it is possible to observe that the velocity scalar field was not well defined near the gurney due to a too coarse mesh in the proximity of the flap trailing edge.

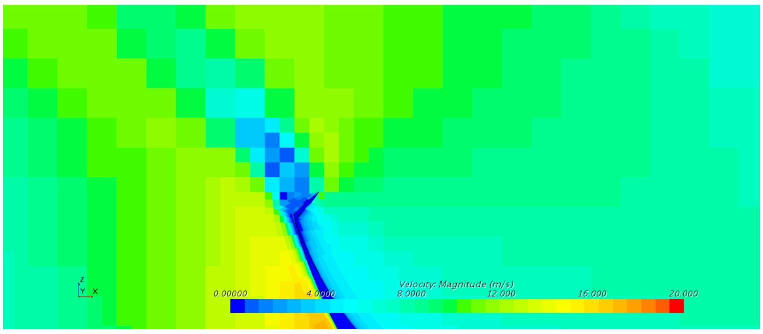

Figure 5.17: *Detail of velocity scalar field near gurney*

5.8 FIFTH ATTEMPT

At this point another detail was added to the geometry: according to the rules [1] there must be a firewall that separates the driver compartment from all components of the fuel supply, the engine oil, the liquid cooling systems and any high voltage system. This component was initially not included in the CFD geometry and it was added in this attempt.

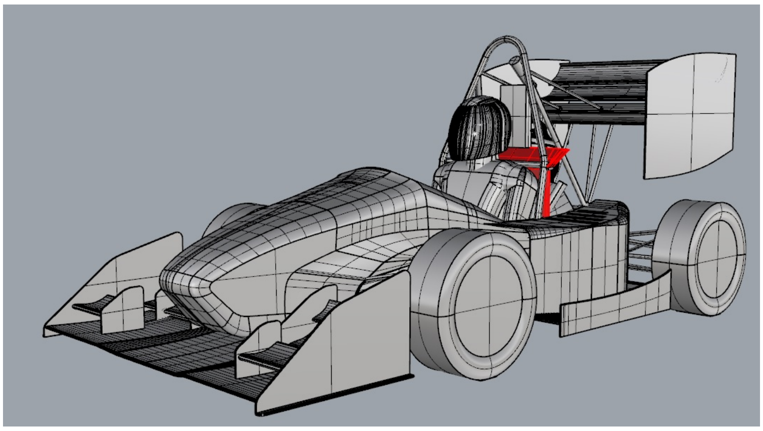

Figure 5.18: *Modified geometry with firewall*

Moreover the mesh, especially near the rear wing and in the wake region, was modified with new volumetric refinement; the control used are visible inFigure5.19 and are listed below:

- Gurney
- Driver cell
- Airbox
- Rear wing pressure side and wake
- Car wake

- Radiator

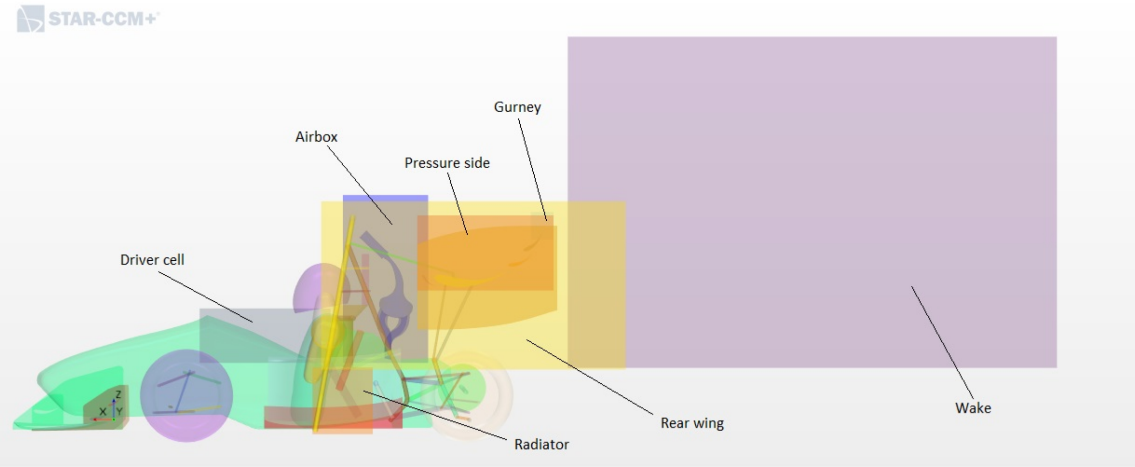
STAR-CCM+
Gurney
Airbox
Pressure side
Driver cell
Rear wing
Wake
Radiator

Figure 5.19: *Volumetric refinement*

The idea was to create a finer mesh near the car that gradually grew moving away from the surfaces using several parallelepipeds, with increasing dimension, in order to define the control volumes. Additionally, a specific volumetric control for the gurney was determined (Figure5.20).

To limit the mesh dimension, the number of boundary layers was lowered to 15 on the wings and to 12 on the rest of the car; in this way the mesh size became 18.7 mln (Figure5.21).

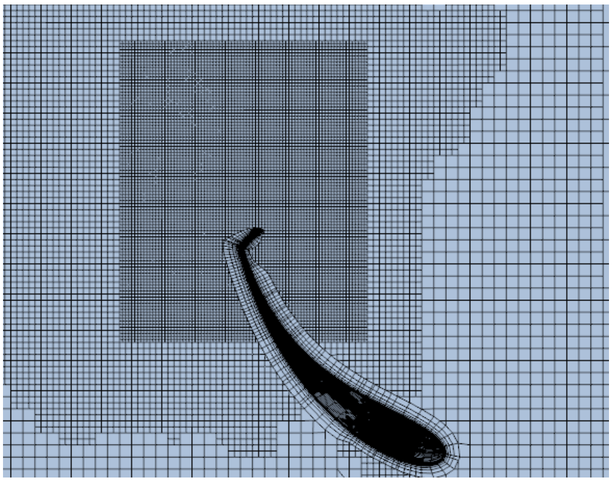

Figure 5.20: *Volumetric refinement at the gurney*

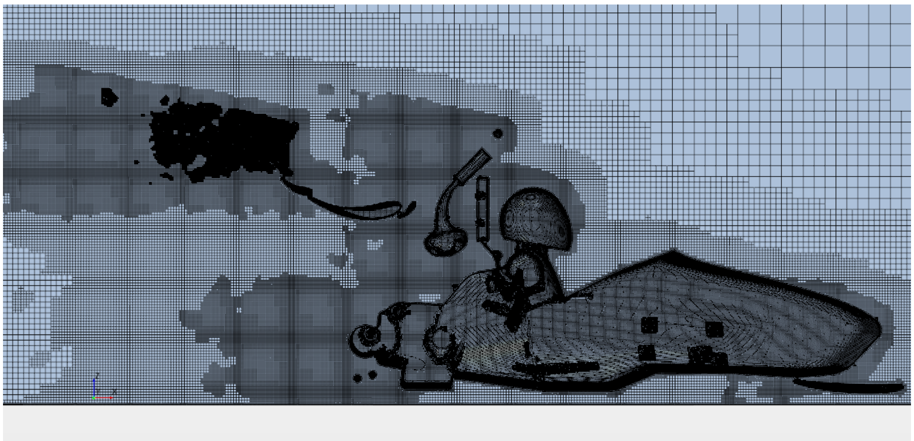

Figure 5.21: *Fifth Attempt mesh*

The simulation results are the following:

	Cl*A	Cd*A	Cl*A error (%)	Cd*A error(%)
Experimental test	0.7865	0.328		
Original mesh	0.896	0.333	13.95	-2.33
First Attempt	1.048	0.387	33.22	13.51
Second Attempt (y+ improvement)	1.039	0.374	32.05	9.81
Third Attempt (wake refinement)	1.004	0.359	27.68	5.35
Fourth Attempt (gurney)	1.079	0.400	37.2	17.3
Fifth Attempt (firewall)	0.647	0.318	-16.22	1.01

The firewall produced a serious decrease of the aerodynamic coefficients, underlying the great importance of this component for the aerodynamic performance of the car.

Compared to the previous attempt, the resolution of the velocity scalar field near the gurney was considerably better (Figure5.22).

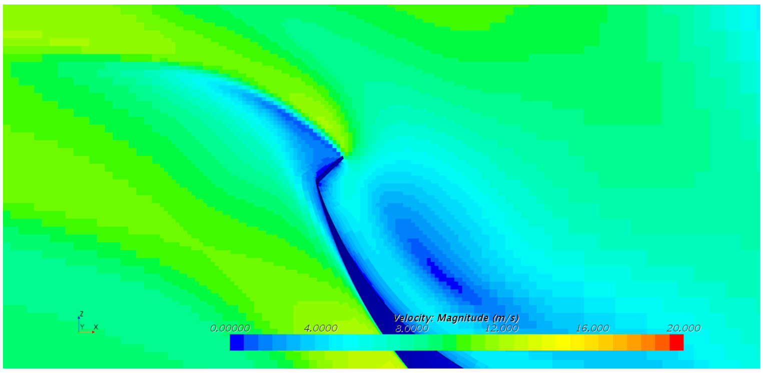

Figure 5.22: *Velocity scalar field at the gurney*

5.9 Sixth Attempt

At this point a different strategy was used. The *wake refinement* approach was abandoned, instead a volumetric controls system was preferred. Therefore, the same volumetric refinements of the previous attempt were enlarged and other two were created near the transmission system and on the underbody region. Various mesh tests were carried out, changing the refinement parameters, in order to obtain a better distribution of the smallest elements and thus improve the resolution of the flow field. The final set-up was based on a larger base size (from 130mm to 180mm) and a lower number of boundary layers (from 12 to 8) bringing the number of elements to 14.7 mln.

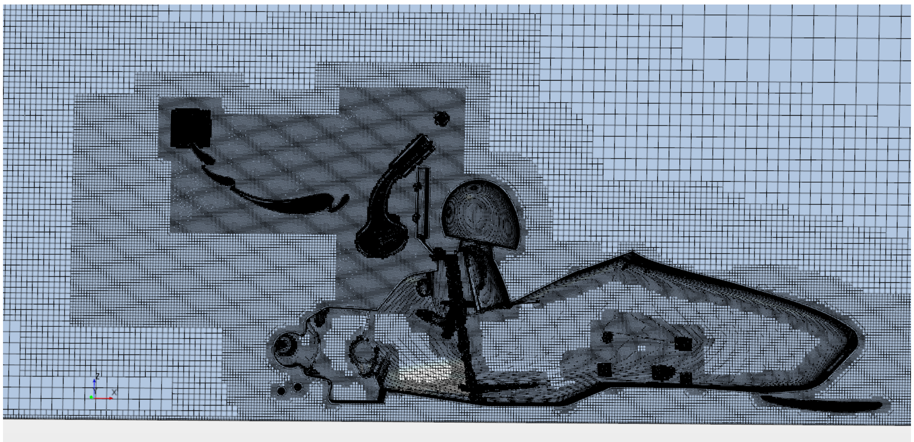

Figure 5.23: *Sixth attempt mesh*

The results obtained from the simulation are the following:

	Cl*A	Cd*A	Cl*A error (%)	Cd*A error(%)
Experimental test	0.7865	0.328		
Original mesh	0.896	0.333	13.95	-2.33
First Attempt	1.048	0.387	33.22	13.51
Second Attempt ($y+$ improvement)	1.039	0.374	32.05	9.81
Third Attempt (wake refinement)	1.004	0.359	27.68	5.35
Fourth Attempt (gurney)	1.079	0.400	37.2	17.3
Fifth Attempt (firewall)	0.647	0.318	-16.22	1.01
Sixth Attempt (Volumetric approach)	0.829	0.335	5.49	-1.77

The errors values are the lowest until this point and considering the margin of error of the experimental test they can be considered acceptable.

5.9.1 MESH SENSITIVITY ANALYSIS

In order to verify if the results found were independent from the mesh, a mesh sensitivity analysis was performed changing the mesh base size. Three different mesh were tested using a base size of 165mm, 150mm and 130mm.

	Base size	Mesh dimension	Cl*A	Cd*A
Fifth Attempt	180	14.7	0.829	0.335
First mesh sensitivity	165	18.2	0.868	0.350
Second mesh sensitivity	150	22.7	0.952	0.364
Third mesh sensitivity	130	29.5	0.672	0.316

Table 5.3: *Sensitivity analysis results*

The results showed how the values from the fifth attempt were mesh dependent and, for this reason, unreliable.

Other tests were performed using the same approach, but different parameters; however stability problems and failure occurred which made the resolution impossible even with various mesh set-up. The reason of these errors was supposed to be the interface between the volumetric refinements and, because of this, the volumetric approach was abandoned.

5.10 SEVENTH ATTEMPT

A different strategy was adopted from this point; for the mesh the $wake\ refinement$ control was improved: the relative base size inside the control volume was reduced (from 200 to 100) and, to avoid too large mesh, the spread angle was reduced (from 20 to 10) because from the previous simulations was noticed that the wake develop was not so extensive. Another relevant change was done on the mesh procedure: to initialize better the solution a step approach was used for the resolution using mesh with different base size, gradually smaller. The procedure adopted is the following:

$$500mm(8.6mln) \Rightarrow 300mm(12mln) \Rightarrow 180mm(22.5mln) \tag{5.1}$$

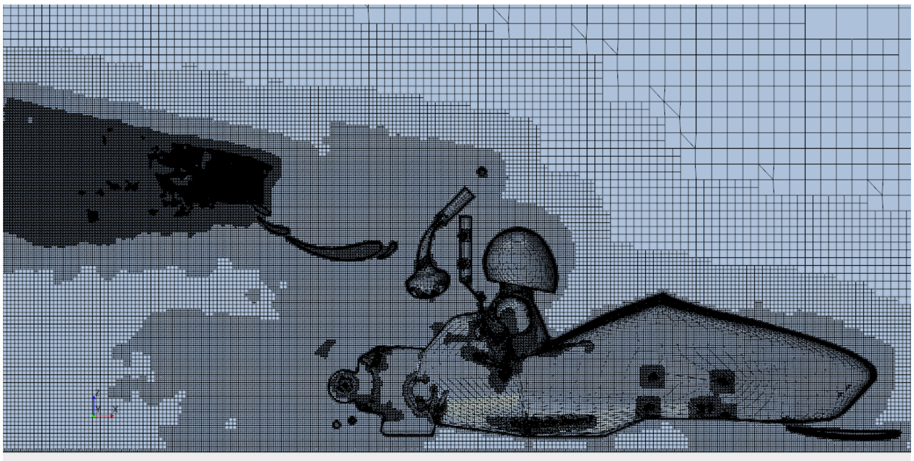

Figure 5.24: *Final mesh*

The first two steps ran for 1000 iterations each, while the third and last step for other 6000 iterations.

	Cl*A	Cd*A	Cl*A error (%)	Cd*A error(%)
Experimental test	0.7865	0.328		
Original mesh	0.896	0.333	13.95	-2.33
First Attempt	1.048	0.387	33.22	13.51
Second Attempt (y+ improvement)	1.039	0.374	32.05	9.81
Third Attempt (wake refinement)	1.004	0.359	27.68	5.35
Fourth Attempt (gurney)	1.079	0.400	37.2	17.3
Fifth Attempt (firewall)	0.647	0.318	-16.22	1.01
Sixth Attempt (Volumetric approach)	0.829	0.335	5.49	-1.77
Seventh Attempt (Mesh steps)	0.785	0.324	-0.15	-4.83

The results (Table**??**) obtained were excellent respect the other attempts, but the residuals (Figure5.25) remained too high even though the force values (Figure5.26) were steady.

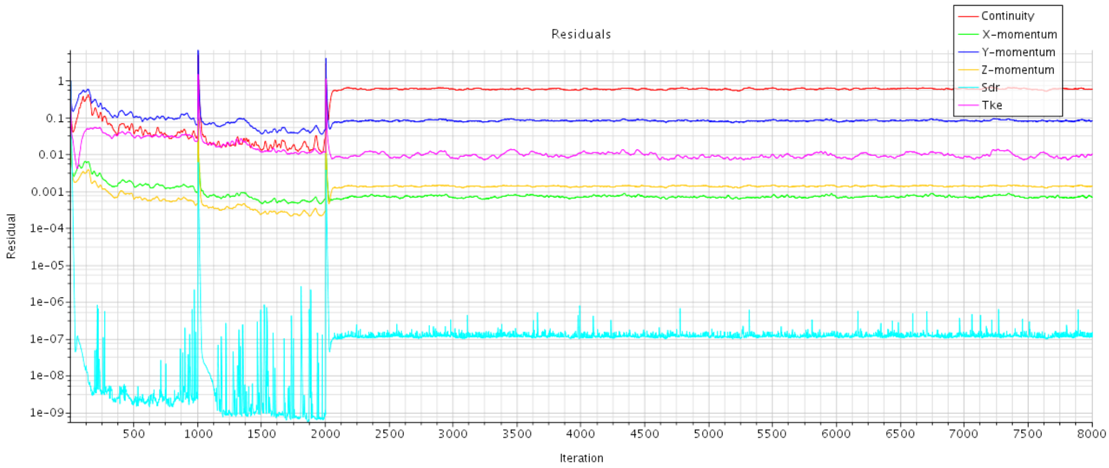

Figure 5.25: *Seventh attempt residuals*

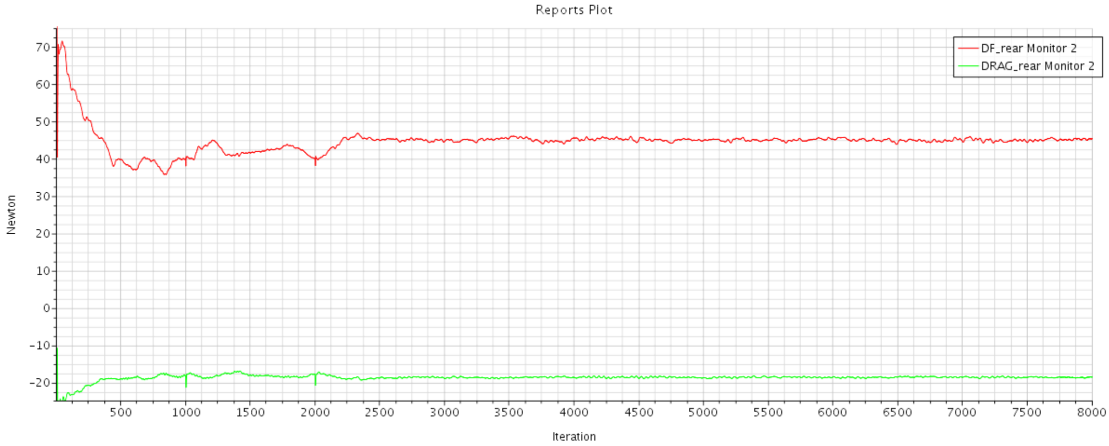

Figure 5.26: *Seventh attempt forces*

The reason for this was deduced to be the intrinsically unsteadiness of the problem; starting from the final iteration of the steady simulation an unsteady analysis was performed.

5.10.1 UNSTEADY ANALYSIS

An unsteady analysis requires the set-up of additional parameters; in particular the $time-step$ defines the time interval to evaluate during the simulation and it has a fundamental role to resolve well the physics of the problem. The $time-step$ was set using the following relation:

$$time-step = 10\frac{\Delta_{min}}{V_0} = 3E-05s \qquad 5.2$$

where Δ_{min} is the minimum cell dimension and V_0 is the flow velocity. For each $time-step$ 25 iterations were performed and the physical time studied was 0.5s.

The results (Table5.4) in terms of forces (Figure5.29) remained similar to the steady analysis and almost all the residuals decrease to acceptable value: the highest was the

	Cl*A	Cd*A
Sixth Attempt (Mesh steps)	0.785	0.324
Unsteady 1 (time-step=3E-05s)	0.796	0.329
Unsteady 2 (time-step=1.5E-05s)	0.785	0.342

Table 5.4: *Results unsteady analysis*

Y-momentum residuals($\approx 8E-04$). The cells with the highest residuals were located after the wake refinement and near the symmetry plane; because of the proximity of the symmetry plane, the reason for the high residuals was supposed to be the presence of cross flow inside the turbulent wake. This effect is visible from the Figure5.27) which shows the y-component of the velocity in a plane section placed behind the car; the two visible spots indicate the presence of cross flow, but the symmetry condition impose a null velocity in y-direction. This conflict can be the explanation for the high residuals.

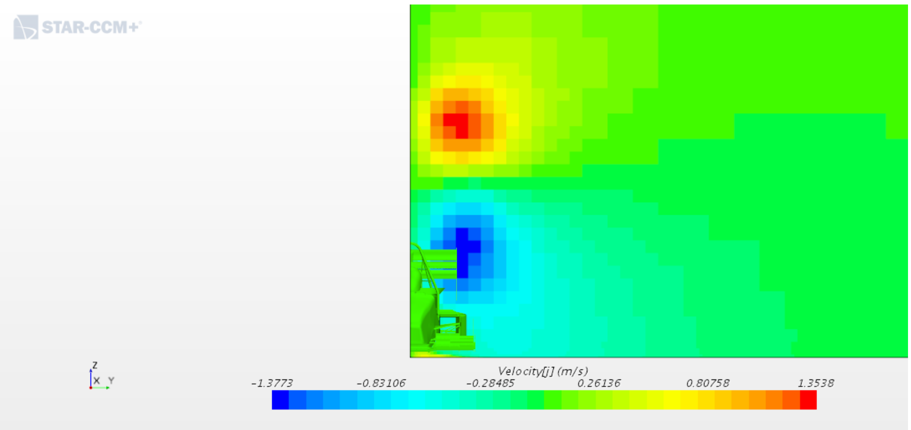

Figure 5.27: *Y-Velocity field in the wake region*

A second unsteady analysis was performed halving the Δt in order to verify the independence of the solution from the $time - step$; the values of the aerodynamic coefficients remained within an acceptable distance from the first simulation.

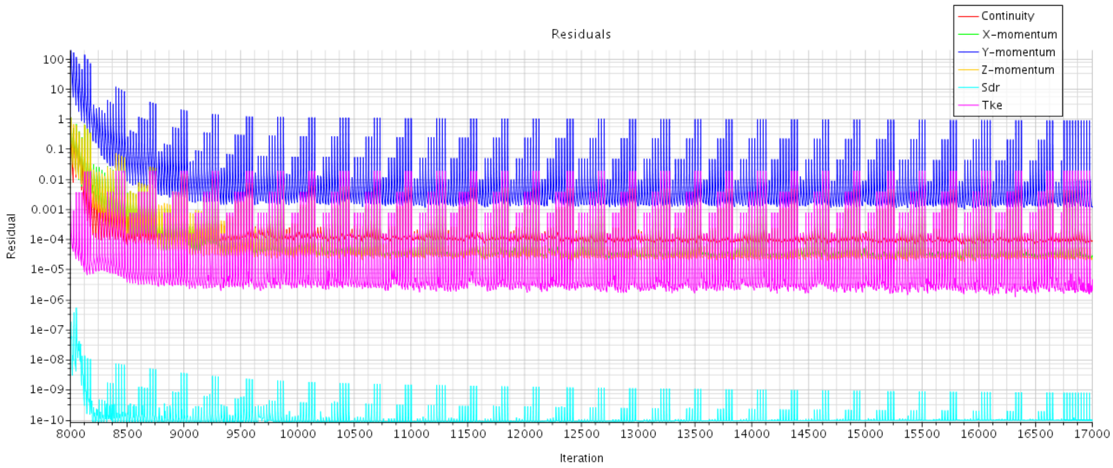

Figure 5.28: *Unsteady analysis residuals*

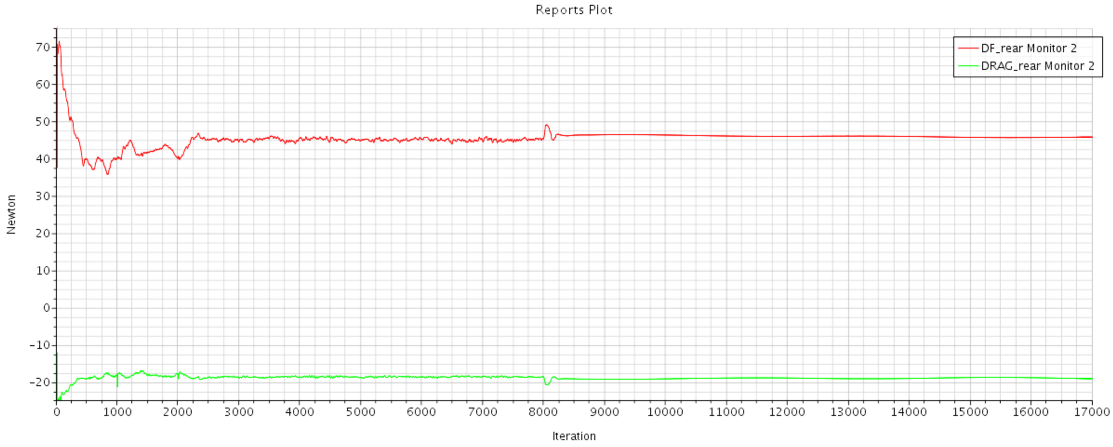

Figure 5.29: *Unsteady analysis forces*

The highest $time - step$ was decided to use in the following analysis because it was less computationally expensive.

5.10.2 MESH SENSITIVITY

A mesh sensitivity investigation on the unsteady analysis was executed, as was done for the previous attempt, changing the final base size. Two different strategies were applied:

- The final mesh step was replaced with lower base size (from 180mm to 165mm and 140mm);
- A fourth mesh step with a lower base size was used after the original three steps.

Results

The second approach produced better results even for highly refined mesh and for both the aerodynamic coefficient. Also higher base size mesh were tested to verify the curve trend of the mesh sensitivity.

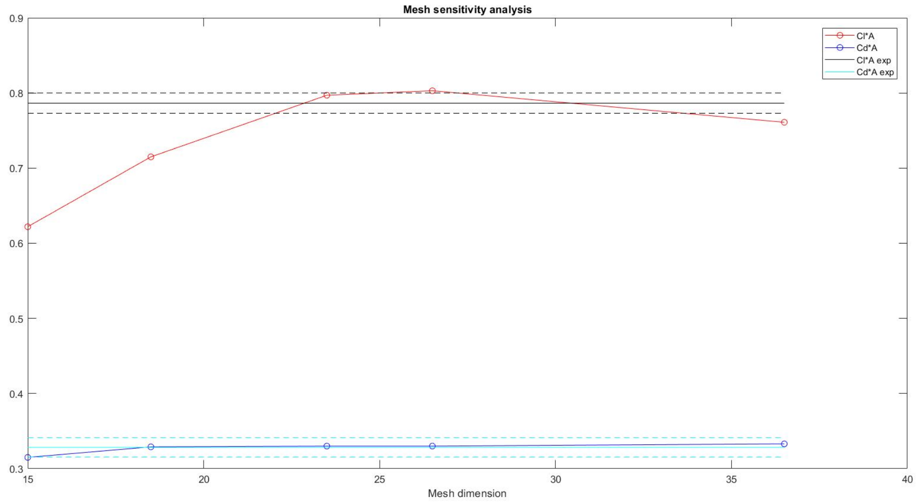

Figure 5.30: *Mesh sensitivity trend curve*

The best base size, as trade-off between mesh dimension and results, was 180 mm that corresponds to a $\approx$ 22.5 mln elements mesh.

5.11 OTHER CONFIGURATIONS

To complete the validation of the model, the other two tested configurations were analysed using the same mesh and solver parameters. Only the volumetric refinement on the gurney was moved following the movement of the trailing edge.

	Cl*A	Cd*A	Error Cl*A(%)	Error Cd*A(%)
Low load set-up	0.482	0.179	-3.19	0.54
Medium load set-up	0.797	0.330	1.30	-3.40
High load set-up	0.851	0.410	-6.57	6.41

Table 5.5: *Results from different configurations*

The results (Table5.5) confirmed the good quality of the model, showing acceptable errors for both the high and low load set-up.

- VI -

Design of experiments

A DOE (design of experiments) analysis on the MG13.18, the new FSAE car of the Univeristy of Padova, was performed. The goal of the DOE was to find a relation between the aerodynamic configuration of the front and rear wing and the aerodynamic performance of the car in order to use the resulting response surface as basis for future development of an aerodynamic active control. Due to the surface response it should be possible to predict the aerodynamic load and balance of the car according to the flaps inclination. The global shape of the MG13.18 is similar to the MGX.15 and thus the same mesh model, validated in the previous chapter, can be used to perform the CFD simulations. In order to prepare the CFD geometry of the MG13.18, the same strategy used for the MGX.15 and described in Chapter 5 was adopted.

6.1 Variables choice

To reduce the necessary computational time only two variables were used: the first describes the relative inclination between the two rear flaps and the second the relative angle between the central flaps of the front wing. Only the two central front flaps (Figure6.1) were considered because, according to the regulation [1], the lateral flaps must satisfy strict geometrical constraints and thus they must be kept fixed.

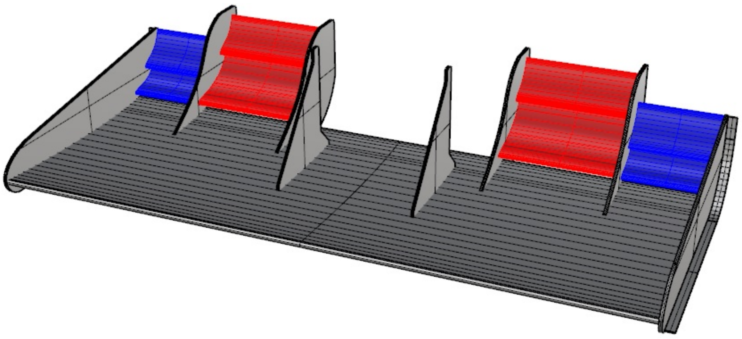

Figure 6.1: *Front wing: in red the central flaps, in blue the lateral flaps*

The flaps are attached to the endplates using two M3 screws per each side; the rearmost point is used as the pivot to change the angle of attack of the profiles. Figure6.2 illustrates the control system: the red circle is the pivot point, while the blue surface and the green line define the range for the angle variation.

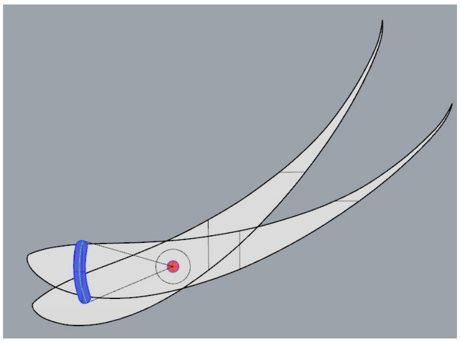

Figure 6.2: *Example of flap rotation*

The relative rotation of both the front and rear flaps is defined using a linear relation: starting from an high load configuration, the profiles inclination was reduced to an half (low load set-up) and then a medium load configuration was defined using an average angle of attack (Figure6.3).

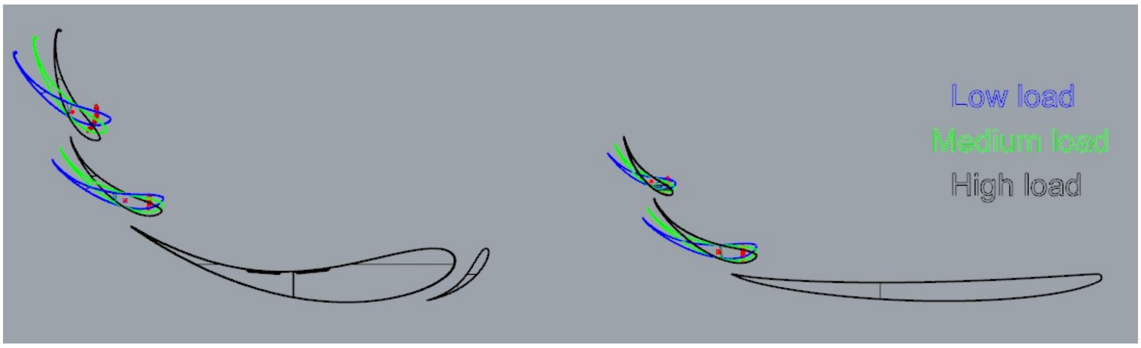

Figure 6.3: *Aerodynamic configurations*

6.2 DOE SET-UP

The DOE analysis was based on a nine-points grid, considering three steps per each variable (Figure6.4).

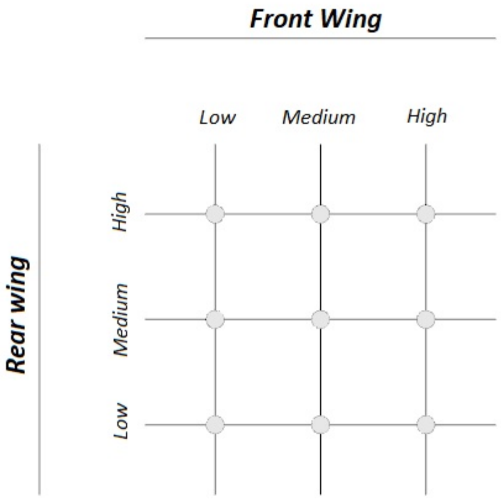

Figure 6.4: *Nine-points grid for the DOE*

	Flap1 (deg)	Flap2 (deg)	
Rear wing	40	70	High Load
	30	52.5	Medium Load
	20	35	Low Load
Front wing	30	50	High Load
	22.5	37.5	Medium Load
	15	25	Low Load

Table 6.1: *Absolute flap inclination for different configurations*

Nine-points are the minimum number of points required in order to obtain an approximate response surface. For each point of the grid a CFD analysis was performed using the same mesh model and the same resolution parameters and strategy adopted for the validated case; this allows to obtain reliable results from the simulations. The inlet velocity chosen for the analysis is 50 km/h.

6.2.1 DOE RESULTS

The results, in terms of downforce and drag of the front wing, rear wing and of the entire vehicle, for each simulation are the following:

RW F1/F2 (deg)	FW F1/F2 (deg)	Rear DF (N)	Rear Drag (N)	Front DF (N)	Front Drag (N)	Tot DF (N)	Tot Drag (N)	Tot Efficiency (DF/Drag)
40/70	30/50	87	45.08	105.14	19.72	187.56	127.92	1.466
20/35	30/50	71.48	29.9	106.62	20.2	167.04	109.22	1.529
30/52.5	30/50	82.72	38.7	105.68	19.94	177.4	118.82	1.493
40/70	22.5/37.5	89.54	46.8	101.28	17.46	183.24	125.74	1.457
40/70	15/25	89.48	45.1	90.36	12.74	170.6	118.48	1.440
30/52.5	22.5/37.5	86.6	37.88	97.96	16.7	173.4	110.82	1.565
30/52.5	15/25	84.5	38.76	89.6	12.56	158.74	109.58	1.449
20/35	22.5/37.5	71.16	29.38	99.72	16.46	161.86	101.32	1.597
20/35	15/25	71.78	29.42	86.88	12.26	143.7	101.22	1.420

Table 6.2: *DOE results*

Analysing these results it is possible to notice that the performance of the rear wing are not highly influenced by the front wing set-ups, at least as concerns the configurations used.

Response surface

The response surface describes the relationships between explanatory variables and one response variable, interpolating the data from the DOE. In this case the explanatory variables were the same used for the DOE analysis (front and rear flaps inclination) and the response variables were the total downforce, the total drag and the car efficiency. In order to represent the surface, a Matlab script was written which reads the data and, using the command *fit*, draws the surface; as a nine-points grid was used for the DOE, a quadratic surface was defined.

Thanks to these surfaces it is possible to evaluate the output forces for an aerodynamic configuration different from the ones simulated; however, in order to obtain better prevision, more points should be used to define the response surface.

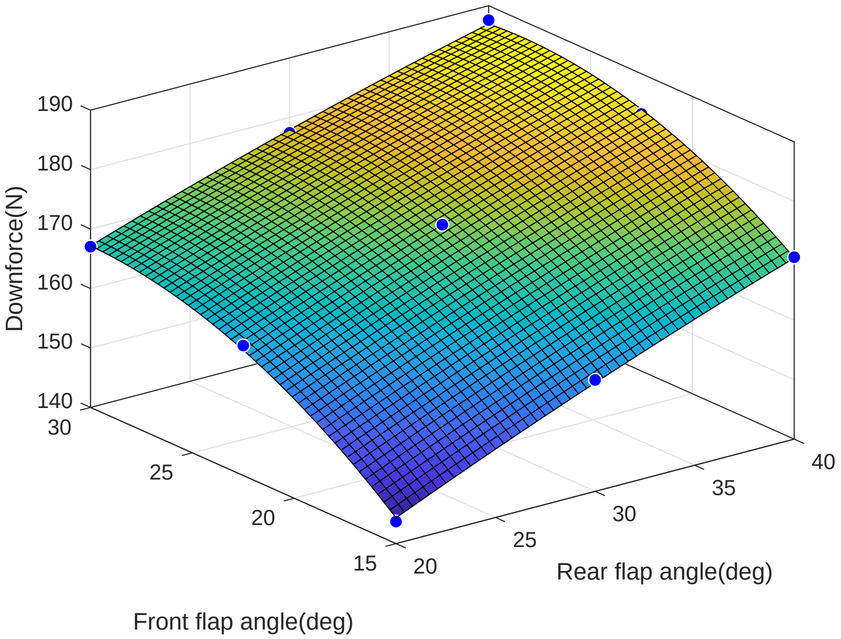

Figure 6.5: *Downforce response surface*

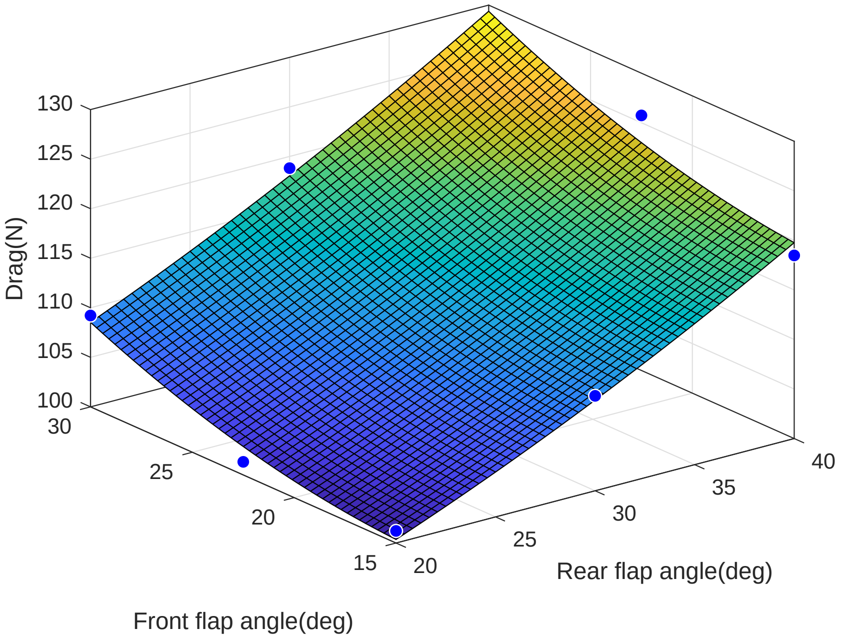

Figure 6.6: *Drag response surface*

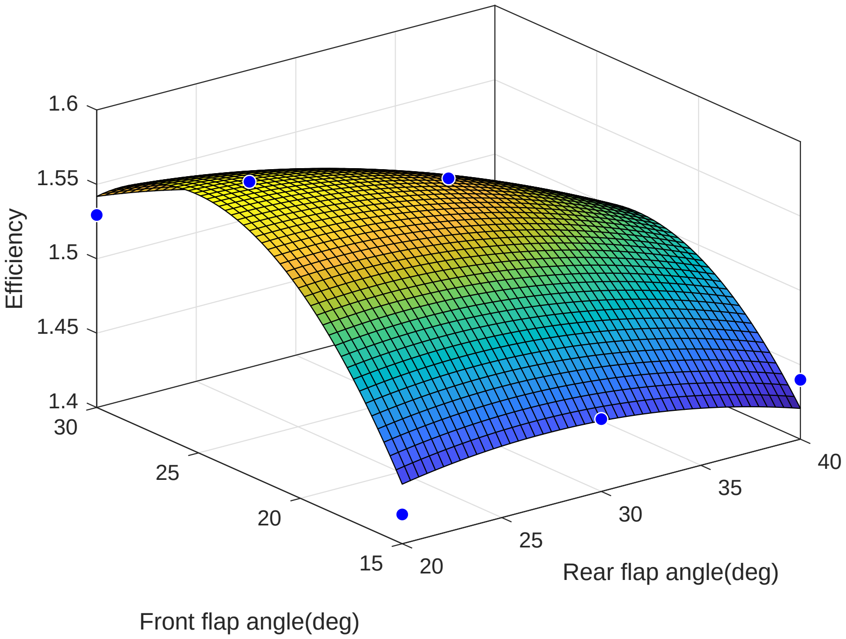

Figure 6.7: *Efficiency response surface*

6.3 AERODYNAMIC BALANCE

An interest result, which is possible to obtain from the DOE, regards the aerodynamic balance and in particular the creation of a response surface that has, as response variable, the aerodynamic load distribution. In order to calculate it, the center of pressure of the car must be found from the DOE results using only mathematical relations.

6.3.1 CENTER OF PRESSURE

The center of pressure of an airfoil is the point where the resultant of all the aerodynamic forces are applied and therefore the resultant moment is zero. The moment of a force is defined as:

$$\vec{M} = \vec{r} \wedge \vec{F} \tag{6.1}$$

where $\vec{r}$ is the distance between the application point of the force and the center of the reference system and $\vec{F}$ is the force resultant. Developing the previous equation the following system is found:

$$\begin{cases} M_x = -F_y z + F_z y \\ M_y = F_x z - F_z x \\ M_z = -F_x y + F_y x \end{cases}$$

Considering the case analysed in this thesis some simplifications can be performed exploiting the symmetry condition:

- the resultant F_y is zero;
- M_x and M_z are zero.

The system is then transformed in:

$$\begin{cases} M_y = F_x z - F_z x \\ y = 0 \end{cases}$$

where F_x is the drag and F_z is the downforce. According to this, it is possible to observe that the system has infinite solutions and thus the center of pressure lays on a line oriented as the force resultant and belonging to the symmetry plane.

In order to find the position of the COP from the simulations performed, the moments around the y-axis and the forces were calculated from the CFD and then, supposing two values for the x-coordinate, the correspondent z-coordinates were found and this allowed to draw the COP line in the CAD file.

Importance of the COP

The position of the COP is fundamental to influence the car behaviour. A vehicle is characterised by a weight distribution which is defined by the position of the components and of the driver relative to the two wheels axles. This characteristic, together with other suspensions set-ups, defines the comportment of the car especially during the turning phase. Three different behaviour can be defined:

- Understeer
- Oversteer
- Neutral

Understeering is the lack of responsiveness of the car front in turning into a corner and it can be caused by a lack of load at the front axle; understeer is inherently stable and thus once the car reduces speed sufficiently the grip will be restored. Oversteering is the tendency of a car rear to slip out in mid-corner, turning front of the car to much in the corner. Oversteer is highly unstable: unless a driver acts to correct it quickly with skilful use of steering and throttle it can cause a spin. However an oversteering car helps the driver to turn and, at the limit of adhesion, it enables a skilled driver to carry far more speed through a corner than understeer.

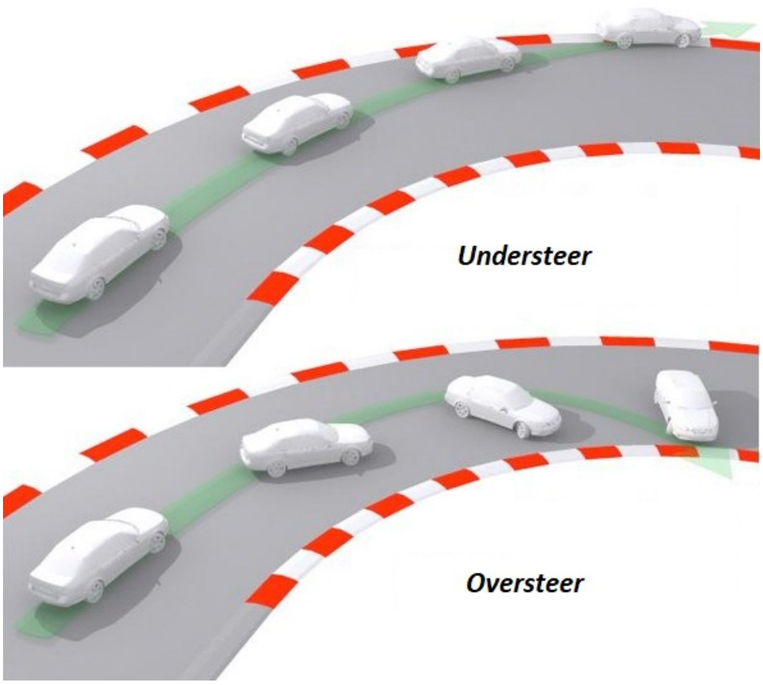

Figure 6.8: *Comparison between understeer and oversteer*

As it is described in Chapter 2 the aerodynamic forces can change the load on the wheels. However, unlike the suspension set-ups and static weight distribution, the magnitude of the aerodynamic forces depends on the velocity squared of the car: at low speed the aerodynamic contribution is smaller and therefore the car behaviour is defined by the static characteristics, while at higher speed the aerodynamic forces growth and therefore their effects become more important until they exceed the statical contribution. If the COP does not coincide with center of gravity of the car, the aerodynamic forces will change the load distribution of the car and its behaviour at high speed. For example an oversteering vehicle at low speed can become an understeering vehicle at high speed if the center of pressure is behind the center of gravity.

6.3.2 Load distribution

In order to obtain the load distribution of the aerodynamic contribution a geometric construction was used. For the MG13.18 the estimate height of the COG is 310mm from the ground and the static load distribution front/rear is 49/51; thanks to this the position of center of gravity is set and it can be drawn on the CAD (Figure6.9).

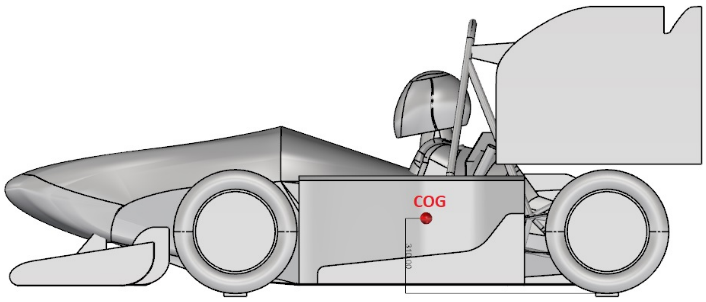

Figure 6.9: *COG position*

As described above, the equation for the COP line was derived from the CFD data and therefore all the lines can be traced respect the same geometry (Figure6.10).

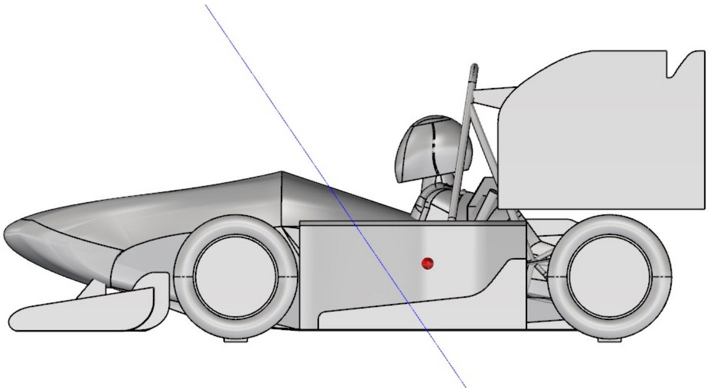

Figure 6.10: *Example of COP line*

To evaluate the load distribution a single point of the COP line must be considered: the point chosen was the intersection point between the COP line and the ground(Figure6.11).

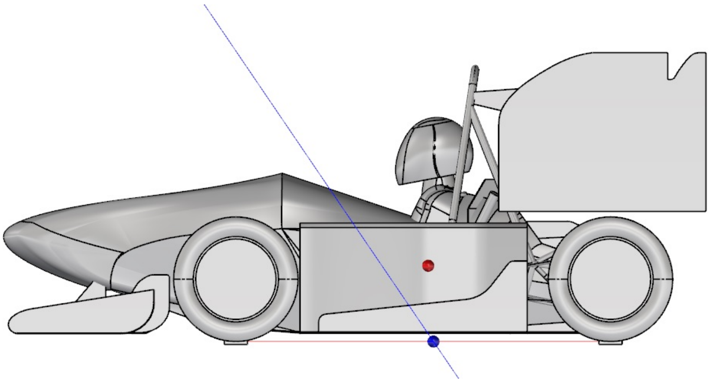

Figure 6.11: *Definition of the COP*

Evaluating the distance between this point and the wheel axles allows to calculate the load distribution using a simple proportion between this measure and the car wheelbase (1535 mm). The results considering all the nine points are the following:

wheelbase=1535mm				
RW F1/F2 (deg)	FW F1/F2 (deg)	Distance from rear axle (mm)	%Front	%Rear
40/70	30/50	812.54	52.93	47.07
20/35	30/50	950.58	61.93	38.07
30/52.5	30/50	820.31	53.44	46.56
40/70	22.5/37.5	750.44	48.89	51.11
40/70	15/25	651.8	42.46	57.54
30/52.5	22.5/37.5	773.85	50.41	49.59
30/52.5	15/25	666.05	43.39	56.61
20/35	22.5/37.5	833.94	54.33	45.67
20/35	15/25	725.68	47.28	52.72

Table 6.3: *Load distribution for all the nine points*

The corresponding response surface is illustrated in Figure6.12.

Thanks to this the load distribution for a continuous range of aerodynamic configuration can be predicted and thus the researched vehicle balance can be obtained.

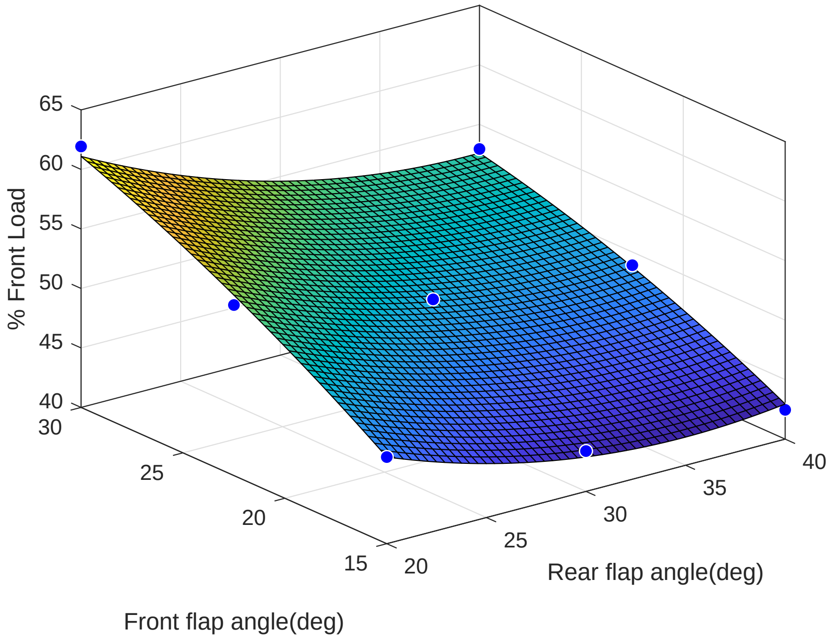

Figure 6.12: *Load distribution response surface*

- VII -

CONCLUSIONS

The validation process allows to obtain a good mesh and a physics model that replies the experimental results within an acceptable error. However more experimental data would be very helpful to create an even more reliable model. For example, additional load values are possible to acquire by:

- testing the front wing with a similar method used for the rear wing and described in Chapter 4;
- using a strain gauges system on suspensions, in order to measure the global vertical forces produced by the car.

Moreover a local validation can further improve the reliability of the results: to do this, many pressure sensors placed on the surfaces, mainly on the rear and front wing, measure the pressure field and thus describe the behaviour of the flow on the wings.

As concerns the geometry preparation, it was noticed that it is very important to determine which elements have a meaningful effect on the flow field; identifying the most influencing components allows to obtain more reliable results in less time. Moreover the sensitivity analysis on the mesh is fundamental to understand the validity of the model and to find the best trade-off in terms of accuracy and computational time required.

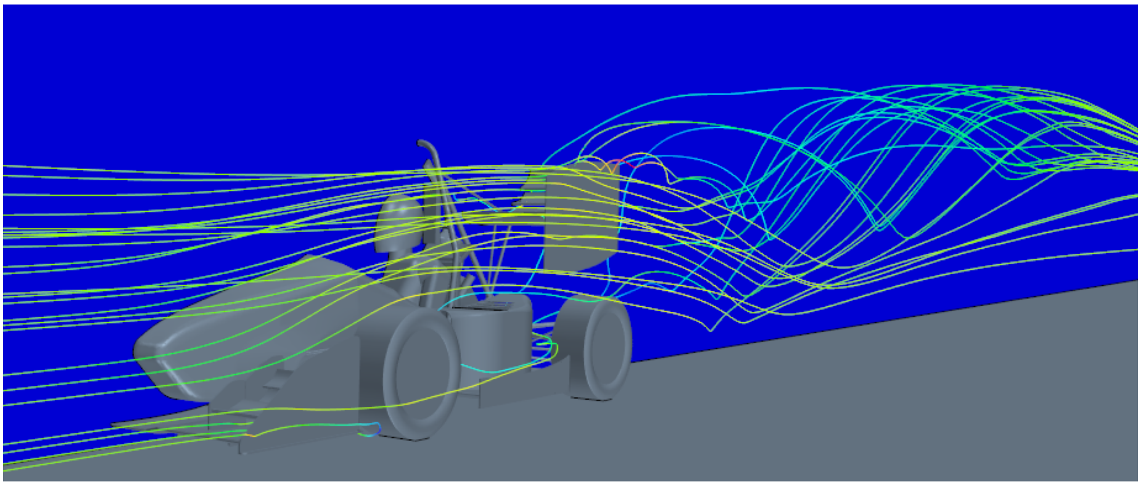

The DOE analysis permits the creation of a response surface, which can be used not only for the aerodynamic set-up of the car, but also as a basis for a future development of an active control of the front and rear flaps. The results show that the front wing has not a great influence on the rear wing performance and they almost exhibit an independent behaviour.

According to this, the set-up of the aerodynamic configuration is easier because the modifications at the front do not affect the rear wing and thus the control system can consider the two element separately.

However better results can be obtained using a larger and more populated grid: for example a sixteen-points grid can allow the definition of a more precise response surface keeping the same angle variations or enlarging the ranges of the variables describing a larger solution space.

BIBLIOGRAPHY

[1] *2017-2018 Formula SAE Rules.* SAE International, 2017.

[2] Joseph Katz. Race car aerodynamics. *Robert Bentley*, 1995.

[3] Wolf-Heinrich Hucho. *Aerodynamik der stumpfen Körper.* Springer, 2002.

[4] Wolf-Heinrich Hucho. *Aerodynamik des Automobils: Strömungsmechanik, Wärmetechnik, Fahrdynamik, Komfort.* Springer-Verlag, 2015.

[5] *User's guide Star ccm+.* CD-Adapco, 2015.

[6] A Cengel Yunus et al. Heat transfer: a practical approach. *MacGraw Hill, New York*, 2003.

[7] *Law of the wall.* Wikipedia.org.

[8] Henk Kaarle Versteeg and Weeratunge Malalasekera. *An introduction to computational fluid dynamics: the finite volume method.* Pearson Education, 2007.

[9] Marco De Lazzari. *Acquisizione e analisi dei carichi aerodinamici all'ala posteriore della vettura formula SAE Mg 10.15.* University of Padova, 2017.